The Abdus Salam
International Centre for Theoretical Physics

United Nations
Educational, Scientific and
Cultural Organization

IAEA
International Atomic Energy Agency

2152-26

Joint ICTP-IAEA Course on Natural Circulation Phenomena and Passive Safety Systems in Advanced Water Cooled Reactors

17 - 21 May 2010

LOCAL PHENOMENA ASSOCIATED WITH NATURAL CIRCULATION

Saha Dilip presented by P.K. Vijayan
Reactor Engineering Division
Bhabha Atomic Research Centre Trombay
Mumbai
India

IAEA Training Course on Natural Circulation Phenomena and Passive Safety Systems in Advanced Water-Cooled Reactors, ICTP, Trieste, Italy, 17-21 May 2010

Lecture Notes T4 and T5

on

LOCAL PHENOMENA ASSOCIATED WITH NATURAL CIRCULATION

by

Dilip Saha

Reactor Engineering Division, Bhabha Atomic Research Centre
Trombay, Mumbai-400085, INDIA

May 2010

LOCAL PHENOMENA ASSOCIATED WITH NATURAL CIRCULATION

Dilip Saha

Reactor Engineering Division, Bhabha Atomic Research Centre, Trombay, Mumbai-400 085, India

E-mail : dsaha@barc.gov.in

KEYWORDS

Natural circulation phenomena, thermohydraulic relationships, non-condensable gases

LECTURE OBJECTIVES

The objective of this lecture is to impart to the participants an adequate knowledge of various phenomena encountered in the natural circulation systems of a nuclear reactor. All the components of the primary system of a nuclear reactor are described and phenomena occurring in each of them are explained. A comprehensive coverage of related thermohydraulic relationships is provided which will enable the participants to carryout the process design of a natural circulation system.

1. INTRODUCTION

In nuclear reactors, natural circulation is increasingly being used for passive heat removal from core under both accidental and normal operating conditions. Natural circulation in a closed loop is established by locating the heat sink at an elevation higher than the heat source. The circulating fluid removes heat from source and transports it to the sink. The flow can be single phase or two phase wherein vapor flows alongside the liquid. These loops are widely used in energy conversion systems. A rectangular closed loop is shown in Figure1. Important phenomena and parameters relevant to the natural circulation loop are discussed below.

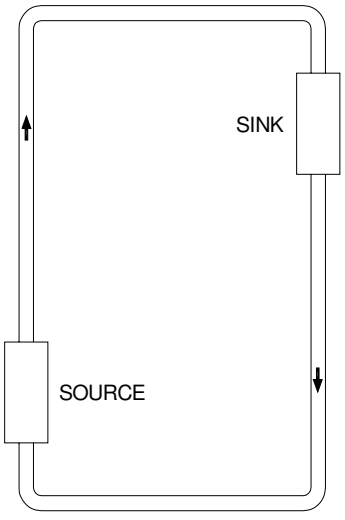

FIG. 1. A rectangular closed natural circulation loop.

1.1. Natural circulation flow rate

Natural circulation flow rate in the loop, under steady state condition is determined from the balance between the driving and the resisting forces. Driving force results from density difference between hot leg and cold leg of the loop. The resisting force is due to pressure losses in the system. The balance of forces can be expressed as:

$$\Delta P_d = \Delta P_f + \Delta P_l + \Delta P_a \quad (1)$$

$$\text{where } \Delta P_d = g \oint \rho dz \quad (2)$$

The above expression indicates that the parameters of interest to determine flow rate are:

a) Single phase and two phase **density**
b) Single and two phase **pressure loss components**

It may be noted that since the driving force in a natural circulation loop is small, it is necessary to minimize and determine very accurately the pressure loss components.

1.2. Heat transfer in source

Figure 2 shows a simple configuration of a cylindrical fuel rod concentrically located inside a circular channel, heat being removed from the rod by coolant flowing through the annulus. Resistance to heat transfer from rod to coolant is mainly restricted to a thin layer of fluid adjacent to rod surface commonly called as film.

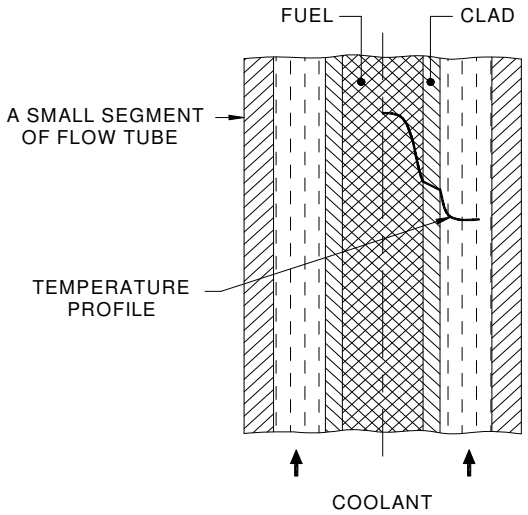

FIG. 2. Radial temperature distribution in fuel and coolant.

Heat transfer from rod to coolant is governed by the Newton's Law:

$$q = h (T_w - T_b) \quad (3)$$

This expression underscores the importance of the **film heat transfer coefficient**, h, in determining the fuel surface temperature and in turn the fuel center temperature.

The maximum heat flux achievable in fuel is mainly limited by **Critical Heat Flux** (CHF). It is characterized by sudden rise in surface temperature at this flux level. At CHF, one of the following two phenomena is encountered:

a) Departure from Nucleate Boiling (DNB)

b) Dryout

1.3. Heat transfer in sink

In Pressurized Water Reactor (PWR) and Pressurized Heavy Water Reactor (PHWR), primary coolant that removes heat from fuel, transports it to steam generator. In steam generator, primary coolant transfers heat to secondary fluid, which starts **boiling.** Thus in the primary side of steam generator coolant temperature reduces without phase change whereas in the secondary side phase change takes place. Steam produced in the secondary side is ultimately condensed in the condenser. Fig. 3 depicts a simplified sketch of a steam generator.

In Boiling Water Reactor (BWR), primary coolant itself boils in the core and the steam, after passing through turbine, is led to condenser where **condensation** of steam takes place. A simplified sketch of a condenser is shown in Fig. 4.In new generation of reactors, a large water pool is being used as heat sink for core decay heat as well as heat released into containment (Fig. 5). **Thermal stratification** in the pool is an important phenomenon which influences heat transfer to the pool to a great extent.

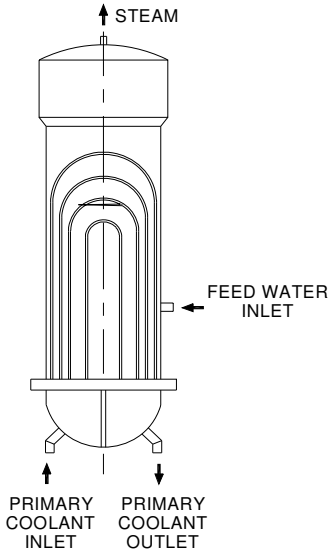

FIG. 3. Steam generator.

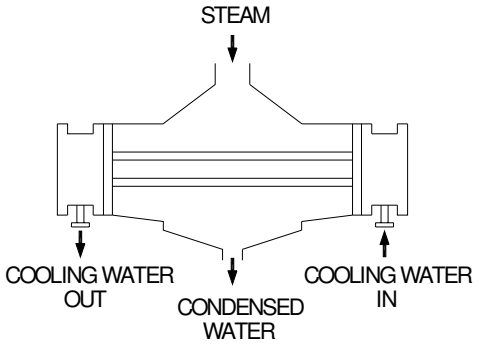

FIG. 4. Condenser.

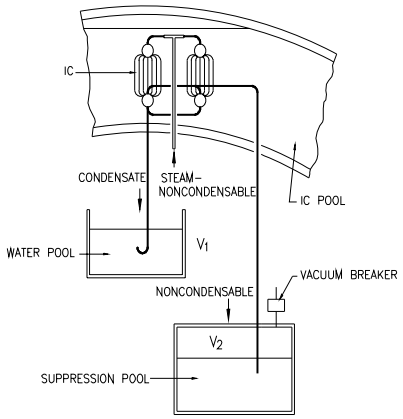

FIG 5. Isolation condenser immersed in a large water pool

Figure 6 depicts a block diagram of all the important phenomena / parameters related to natural circulation discussed so far. These parameters are further discussed in more details in the following sections. A number of correlations given in the following sections are derived based on experimental data generated with forced circulation. Though in most of the cases these correlations can be used for natural circulation, applicability of these correlations for natural circulation should be judiciously checked when secondary flows are present like natural circulation through large diameter pipe at low Reynolds number.

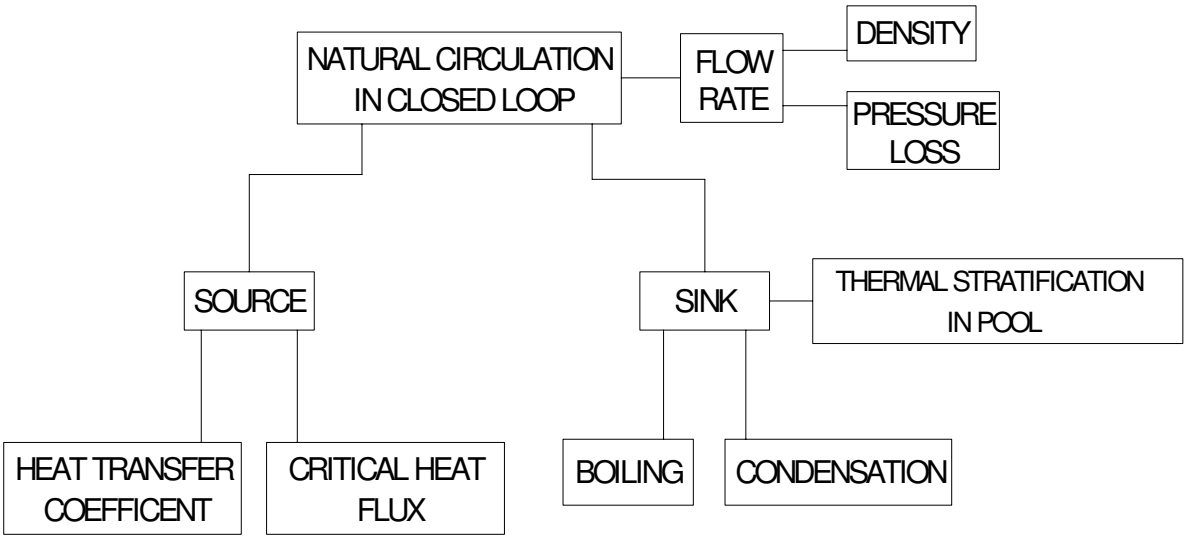

FIG. 6. Important phenomena/ parameters relevant to natural circulation in closed loop.

2. NATURAL CIRCULATION FLOW RATE

2.1. Density

For single phase flow, the density of fluid can be predicted reasonably well with established relationships for thermophysical properties of fluid [1]. For two phase flow the density of two phase mixture at any cross section in the flow path is given by the following equation:

$$\rho = \alpha \rho_G + (1-\alpha)\rho_L \tag{4}$$

The above expression indicates that for two phase flow, it is necessary to predict void fraction accurately to determine density.

2.1.1. Void fraction

Figure 7a depicts upward two phase flow through a vertical channel. Figure 7b shows the flow pattern based on the assumption that the two phases are artificially segregated. Quality (x) at any cross section can be defined as

$$x = \frac{\text{Mass flow rate of vapor}}{\text{Mass flow rate of vapor} + \text{Mass flow rate of liquid}}$$

Void fraction at any cross section is defined as

$$\alpha = \frac{\text{Cross section area occupied by vapor}}{\text{Total channel cross section area}}$$

In general, the void fraction correlations can be classified into following categories:

(a) slip ratio models,
(b) Kβ models and
(c) correlations based on the drift flux model.

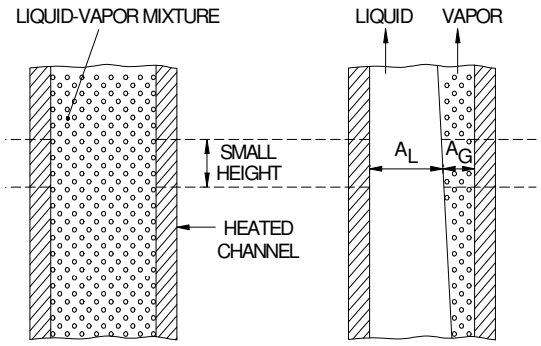

(a) **(b)**

*FIG. 7. Two phase flow in a vertical heated **c**hannel.*

In addition, there are some empirical correlations, which do not fall in any of the three categories. Some of the commonly used correlations in all the above categories are described below.

a) Slip ratio models

These models essentially specify an empirical equation for the slip ratio, S ($=u_G/u_L$). The void fraction can, then be calculated by the following equation:

$$\alpha = \frac{1}{1+\left(\frac{1-x}{x}\right) S \frac{\rho_G}{\rho_L}} \tag{5}$$

For homogeneous flow, $u_G = u_L$ and S = 1. At high pressure and high mass flow rates the void fraction approaches that of homogeneous flow, and can be calculated by setting S = 1 in the above equation. But usually, the slip ratio is more than unity for both horizontal and vertical flows. A commonly used slip ratio model is given below as an example.

Modified Smith [2]

$$S = K + (1-K)\left\{\frac{\frac{\rho_L}{\rho_G} + K\left(\frac{1}{x}-1\right)}{1+K\left(\frac{1}{x}-1\right)}\right\}^{0.5} \tag{6}$$

where K = 0.95 tanh(5.0x)+0.05

b) Kβ models

These models calculate α by multiplying the homogeneous void fraction, β, by a constant K.

Armand's model is given below as an example.

Armand [3]

$$K = 0.833 + 0.167x \tag{7}$$

c) Correlations based on the drift flux model

By far the largest number of correlations for void fraction reported in the literature are based on the drift flux model. The general drift flux formula for void fraction can be expressed as

$$\alpha = \frac{j_G}{C_0[j_G + j_L] + V_{Gj}} \tag{8}$$

where,

V_{Gj} is the drift velocity (= u_G - j, where j is the mixture velocity) and for homogeneous flow C_0 = 1 and V_{Gj} = 0. The various models (IAEA, 2001) [4] in this category differ only in the expressions used for C_0 and V_{Gj} which are empirical in nature.

The Chexal and Lellouche [5] correlation is applicable over a wide range of parameters and can tackle both co-current and counter-current steam-water, air-water and refrigerant two-phase flows. Details of this and some other commonly used correlations can be obtained from IAEA-TECDOC-1203 [4].

2.2. Components of pressure drop

As mentioned earlier in section 1.1, the total pressure loss, Δp comprises of three components, viz. ΔP_f, ΔP_l and ΔP_a which are components of pressure drop due to skin friction, form friction (also known as local friction) and acceleration respectively. The skin friction pressure drop is also known simply as friction pressure drop.

For the purpose of design of advanced reactors, the required correlations mainly cover the following configurations. For friction pressure loss, circular pipe, annulus and rod cluster and for local pressure loss, spacer, bottom and top tie plates, flow area changes like contraction, expansion, bends, tees, valves etc., are most common. In addition, in-core effects like radiation induced creep, blister formation, swelling, corrosion, etc. are also important factors affecting the pressure drop which are not dealt with here. A few pressure drop correlations for different components are given as examples in the following sections. These are described configuration-wise.

2.2.1. Friction pressure drop

This is the irreversible component of pressure drop caused by shear stress at the wall and can be expressed as:

$$\Delta p_f = \frac{fL}{D_h}\frac{W^2}{2\rho A^2} \tag{9}$$

where D_h is equal to 4 times flow area / wetted perimeter.

The pressure drop occurs all along the length and hence referred to as distributed pressure drop sometimes. This equation is applicable for single-phase and homogeneous two-phase flows, although, the method of calculation of the friction factor, f and density, ρ differ in the two cases. Pressure drop across tubes, rectangular channels, annuli, bare rod bundle (i.e. without spacers), etc., are examples of this component. Correlations commonly used to determine friction factor f is discussed below. The following pressure drop correlations are applicable to steady state fully developed flow.

Circular pipe

a) Adiabatic single-phase flow

For fully developed laminar flow, the friction factor is given by:

$$f = 64 / Re \tag{10}$$

which is valid for Reynolds number less than 2000. For turbulent flow in smooth pipes several friction factor correlations are proposed and in use. A few commonly used correlations for smooth pipe are given below.

Blasius [6] proposed the following equation:

$$f = 0.316\, Re^{-0.25} \tag{11}$$

valid in the range $3000 \leq Re \leq 10^5$. The following equation valid in the range of $3000 \leq Re \leq 10^6$ is also often used for design.

$$f = 0.184\, Re^{-0.2} \tag{12}$$

Colebrook [7] proposed the following equation:

$$\frac{1}{\sqrt{f}} = 0.86 \ln\left(\frac{e/D}{3.7} + \frac{2.51}{Re\sqrt{f}}\right) \tag{13}$$

valid for smooth and rough pipes for the whole range of Reynolds number above 3000. The following explicit equation proposed by Filonenko [8] is a good approximation of Colebrook equation for smooth tube in the range $4 \times 10^3 \leq Re \leq 10^{12}$.

$$f = [1.82 \log(Re) - 1.64]^{-2} \tag{14}$$

It may be noted from the above that well established correlations for friction factor do not exist in the transition region between $2000 \leq Re \leq 3000$. A simple way to overcome this problem is to use the following criterion for switch over from laminar to turbulent flow equation.

$$\text{If } f_t > f_l \text{ then } f = f_t \tag{15}$$

where f_t and f_l are friction factors calculated by turbulent and laminar flow equations respectively.

b) Diabatic single-phase flow

Generally isothermal friction factor correlations are used with properties evaluated at the film temperature $T_f = 0.4\,(T_W - T_b) + T_b$, where T_W and T_b are the wall and bulk fluid temperatures [9]. Sometimes the friction factor for non-isothermal flow is obtained by multiplying the isothermal friction factor with a correction coefficient, F. The following empirical equation proposed by Leung and Groeneveld [10] is given as an example

$$F = (\mu_b/\mu_w)^{-0.28} \quad (16)$$

Where the subscripts b and w refer to the bulk fluid and wall respectively.

c) Adiabatic two-phase flow

A large number of two-phase flow pressure drop correlations can be found in literature. These correlations can be classified into the following four general categories.

(1) Empirical correlations based on the homogeneous model,
(2) Empirical correlations based on the two-phase friction multiplier concept,
(3) Direct empirical models,
(4) Flow pattern specific models.

Correlations in the first two categories are given below.

Homogeneous flow model

In the homogeneous flow model, the two-phase frictional pressure gradient is calculated in terms of a friction factor, as in single-phase flow. The friction factor is calculated using one of the equations given for single phase flow in Section 2.2.1(a), with the use of the two-phase viscosity in calculating the Reynolds number. A typical model for two-phase viscosity is given below.

Cicchitti [11]

$$\mu = x\,\mu_G + (1 - x)\,\mu_L \quad (17)$$

Correlations based on the multiplier concept

In this case, the two-phase pressure drop is calculated from the single-phase pressure drop by multiplying with a two-phase friction factor multiplier. The following definitions of two-phase friction multipliers are often used.

$$\phi_{LO}^2 = \frac{(dp/dz)_{TPF}}{(dp/dz)_{LO}}; \quad \phi_{GO}^2 = \frac{(dp/dz)_{TPF}}{(dp/dz)_{GO}};$$

$$\phi_L^2 = \frac{(dp/dz)_{TPF}}{(dp/dz)_L} and \phi_G^2 = \frac{(dp/dz)_{TPF}}{(dp/dz)_G} \quad (18)$$

Where the denominators refer to the single-phase pressure gradient for flow in the same duct with mass flow rates corresponding to the mixture flow rate in case of ϕ_{LO}^2 and ϕ_{GO}^2 and individual phases in case of ϕ_L^2 and ϕ_G^2. Among these, ϕ_{LO}^2 is the most popular friction multiplier. An illustrative multiplier based correlation is given below.

Lottes-Flinn [12]

Correlation for annular upward flow through heated channels is

$$\phi_{LO}^2 = \left(\frac{1 - x}{1 - \alpha}\right)^2 \quad (19)$$

Martinelli – Nelson [13] is a commonly used correlation in this category.

d) Diabatic two-phase flow

The correlations discussed so far are applicable to adiabatic two-phase flow. The effect of heat flux on two phase pressure drop has been studied by Leung and Groeneveld [14], Tarasova [15] and Koehler and Kastner [16]. Tarasova observed that two phase friction pressure drop is higher in a heated channel compared to that in an unheated channel for same flow condition. However, Koehler and Kastner concluded that two phase pressure drops are same for heated and unheated channels. Studies conducted by Leung and Groeneveld indicate that the surface condition is significantly influenced by heat flux. Effective surface roughness increases due to the formation of bubbles at heated surface leading to larger pressure drop. They concluded that for the same flow conditions, the two phase multiplier is larger for low heat flux than high heat flux. The discussions indicate that there is not yet any well-established procedure to take the affect of heat flux into account. However some alternate approaches are suggested in IAEA-TECDOC-1203 [4].

Annulus

Correlations for circular pipe are normally used for the calculation of single phase pressure drop in annulus using the hydraulic diameter concept. For two-phase pressure drop, the same concept is expected to be applicable.

ROD BUNDLE

The rod bundle geometries used in advanced designs differ in several ways. In PWRs and BWRs, the fuel bundles are long (1.8 to 4.5 m approx.) whereas in PHWRs short fuel bundles of about 0.5 m are used. Generally grid spacers are used in PWRs and BWRs while split-wart spacers are used in PHWRs. In certain fast breeder reactors wire-wrapped bundles are still used. In PWRs and BWRs, the total pressure drop is obtained by summing up the pressure drop in bare rod bundle and the spacers. For wire-wrapped bundles empirical correlations for the pressure drop in the bundle considering the geometric details of the wire wraps are available. For PHWR type bundles, the total pressure drop is sometimes expressed in terms of an overall loss coefficient due to the closeness of the spacers and the complex geometry of the end plates [17] and alignment problem at the junction between two bundles [18].

Wire wrapped rod bundles

In the case of wire wrapped rod bundles, the geometry and shape of the system is quite rigid and the development of a general correlation for predicting the pressure drop is a reasonable task. Such a correlation proposed by Rehme [19], [20] is given below:

$$\Delta P = f_R \frac{L}{D_h} \frac{\rho u_R^2}{2} \frac{U_B}{U_G} \tag{20}$$

where

$U_B = U_S + U_D$ is the bundle perimeter

$U_G = U_S + U_D + U_K$ is the total perimeter

U_K, U_S and U_D are the shroud perimeter, pins perimeter and wire perimeter respectively. The reference velocity, u_R, is defined as:

$$u_R = u \sqrt{F}$$

where u is the average velocity in the rod bundle.

The geometrical factor F depends on the pitch to diameter ratio and on the ratio between the mean diameter and the wire pitch (H).

$$F = \left(\frac{p_t}{D}\right)^{0.5} + \left[7.6\frac{d_m}{H}\left(\frac{p_t}{D}\right)^2\right]^{2.16} \quad (21)$$

where d_m is the mean diameter of wire wraps. The reference friction factor f_R is calculated by means of the following correlation based on Rehme's experimental data.

$$f_R = \frac{64}{Re_R} + \frac{0.0816}{Re_R^{0.133}} \qquad \text{for } 2 \times 10^3 \le Re_R \le 5 \times 10^5 \quad (22)$$

where

$$Re_R = Re\sqrt{F} \text{ and } Re = (u_R D_h)/\nu \quad (23)$$

These are valid in the range $1.12 < p_t/D < 1.42$ and $6 < H/dm < 45$.

Bare rod bundles

Single-phase

Correlations for circular pipes are commonly used to calculate pressure drop using hydraulic diameter of the rod bundle in the absence of experimental data. One of the commonly used correlation is:

Kays [21]

$$f = f_{cir} K_1 \quad (24)$$

where

K_1 - is provided as a function of p_t/D (pitch to diameter ratio) based on the work by Diessler and Taylor [22].

f_{cir} - can be calculated using correlations given for circular pipe.

Two-phase

CESNEF-2 [23] correlation is applicable for rod bundles. In addition, there are some empirical equations proposed for rod bundles one of which is given below.

CNEN [24] correlation

$$\Delta p_{TPF} = 1.7205 \times 10^{-6} (L\, M^{0.852}) / D_h^{1.242} \quad (25)$$

M is given by:

$$M = [x v_G + (1-x) v_L] G^2 \quad (26)$$

where M is in $[N/m^2]$, L & D_h are in metres.

Δp_{TPF} is obtained in metres of water at 25°C. This equation is applicable for square array fuel bundles with pitch to diameter ratio = 1.28, D_h = 1.31 cm, peripheral rod-channel gap = 0.55 x pitch, $8 < P < 70$ kg/cm^2 and $680 < G < 2700$ kg/m^{2}s.

2.2.2. Local pressure drop

This is the localized irreversible pressure drop component caused by change in flow geometry and flow direction. Pressure drop across valves, elbows, tee, spacer, etc. are examples. The local pressure drop is given by

$$\Delta p_l = K \frac{W^2}{2\rho A^2} \tag{27}$$

where K is the local loss coefficient, the correlations for which differ for different geometries and for single-phase and two-phase flows.

GRID SPACERS

Because of variation and complexity of geometry, it is extremely difficult to establish a pressure loss coefficient correlation of general validity for grid spacers. But methods of calculation reasonably accurate for design purpose can be achieved. Some correlations used to determine pressure drop across grid spacers are discussed below.

Single-phase flow

Single-phase pressure drop is calculated using a spacer loss coefficient, K, as:

$$\Delta p = K \rho V_B^2 / 2 \tag{28}$$

In some cases, it may be possible to obtain a reasonable value of the spacer loss coefficient if its geometry can be approximated to one of those considered in [25]. For other cases, the different empirical models for K, one of which is described below may be used.

Rehme [26]

$$K = C_v \varepsilon^2 \tag{29}$$

where $\varepsilon = A_g/A_B$.

For $Re_B > 5x10^4$, $C_v = 6$ to 7 and for $Re_B \leq 5x10^4$ C_v values are given in graphical form as a function of Re_B. Subsequently Rehme [27] studied the effect of roughness of rod surface on the pressure drop across spacers. Cevolani [28] proposed $C_v = 5+6133Re^{-0.789}$ for square bundles and $\ln(C_v)=7.690-0.9421 \ln(Re)+0.0379 \ln^2(Re)$ for triangular bundles with an upper limit of K=2 if the calculated value is greater than 2.

Two-phase flow

In general, the homogeneous model or the slip model is used for the estimation of the two-phase pressure drop across grid spacers.

a) Homogeneous model

$$\Delta p = K(Re_{sat}) \, v \, G^2/2 \tag{30}$$

where $K(Re_{sat})$ is the form loss coefficient for single phase flow estimated at the Reynolds number corresponding to the total flow in the form of saturated liquid and v is the specific volume given by

$$v = x \, v_G + (1-x) \, v_L \tag{31}$$

This model may be used when experimental data are not available.

b) Slip model

According to this model, the form loss coefficient for two phase flow can be obtained from

$$\Delta p_{TPF} = \frac{K_{SPF} G^2}{2\rho} = K_{SPF} \frac{\rho_L}{\rho} \frac{G^2}{2\rho_L} = K_{TPF} \frac{G^2}{2\rho_L} \tag{32}$$

where ρ is given by

$$\rho = \alpha \rho_G + (1 - \alpha) \rho_L \; ; \qquad \alpha = \frac{1}{1 + \left(\frac{1 - x}{x} \right) S \frac{\rho_G}{\rho_L}}$$

It may be noted that this equation reduces to the homogeneous model if S = 1. Grillo and Marinelli [29] recommend a value of S = 2 for grid spacers.

Tie plate

Generally, tie plates are used at the ends of rod cluster fuel elements which structurally joins all the fuel pins. Unlike spacers, the flow areas at the downstream and upstream sides of the tie plates are different. Also, these are generally located in the unheated portion of the bundle. Reported studies on pressure drop for the tie plates are few in number. An approximate calculation for design purposes can be made using the contraction and expansion model for local pressure losses. In addition the friction losses in the thickness of the tie plates can be calculated using the hydraulic diameter concept. For two-phase pressure losses, the homogeneous or the slip model described above can be employed in the absence of experimental data.

AREA CHANGES

The single phase pressure losses due to area changes can be calculated by Eqn.(27) with loss coefficients calculated for the relevant geometry from Idelchik [25].

In general, for two phase flow the irreversible pressure drop due to area changes is estimated from the knowledge of single-phase loss coefficient using the homogeneous model. When details of the slip ratio are available, then the slip model given above can be used. Romey (see Ref. [30]) expresses the two-phase pressure drop across sudden expansion by the following equation:

$$\Delta p = G^2 A_r^2 \frac{(1 - A_r)}{\rho_L} \left\{ 1 + x \left(\frac{\rho_L}{\rho_G} - 1 \right) \right\} \tag{33}$$

Bends and fittings

The single-phase pressure drop due to bends and fittings can be calculated using the appropriate loss coefficients from Idelchik [25].

Chisholm and Sutherland [31] provide the following general equation for the calculation of two-phase pressure drop in bends and fittings.

$$\frac{\Delta p_{TP}}{\Delta p_L} = 1 + \left(\frac{\Delta P_G}{\Delta P_L}\right) + C\left(\frac{\Delta P_G}{\Delta P_L}\right)^{0.5} \quad (34)$$

$$C = \left\{1 + (C_2 - 1)\left(\frac{v_{fg}}{v_G}\right)^{0.5}\right\}\left\{\left(\frac{v_G}{v_L}\right)^{0.5}\left(\frac{v_L}{v_G}\right)^{0.5}\right\} \quad (35)$$

where $v_{fg} = v_G - v_L$, and C_2 is a constant**.**

a) Bends

For bends C_2 is a function of R/D, where R is the radius of curvature of the bend and D is the pipe diameter.

R/D	1	3	5	7
C_2 for normal bend	4.35	3.40	2.20	1.00
C_2 for bend with upstream disturbance within 50 L/D	3.10	2.50	1.75	1.00

Chisholm provided the above values of C_2 by fitting Fitzsimmons [32] data.

Chisholm & Sutherland [31]

For 90° bends: $C_2 = 1 + 35\,N$ (36)

For 180° bends: $C_2 = 1 + 20\,N$ (37)

N is the number of equivalent lengths used for calculating single-phase pressure drop.

b) Tees

$C_2 = 1.75$

c) Valves

C_2 = 1.5 for gate valves

= 2.3 for globe valves

Alternatively the homogeneous model may be used.

2.2.3. Acceleration pressure drop

This reversible component of pressure drop is caused by a change in flow area or density. Expansion, contraction and fluid flowing through a heated section are the examples. The acceleration pressure drop due to area change for single-phase and two-phase flow can be expressed as

$$\Delta p_a = \frac{(1 - A_r^2)\,W^2\,\phi}{2\,A_0^2\,\rho_L} \quad (38)$$

where A_0 = smaller flow area. $\phi = 1$ for single-phase flow and for two-phase flow ϕ is given by:

$$\phi = \left(\frac{x^3}{\rho_G^2 \alpha^2} + \frac{(1-x)^3}{\rho_L^2 (1-\alpha)^2} \right) \left(\frac{\rho_G \rho_L}{x \rho_L + (1-x) \rho_G} \right) \quad (39)$$

The acceleration pressure drop due to density change for single-phase and two-phase flows can be expressed as:

$$\Delta p_a = G^2 \left\{ \left(\frac{1}{(\rho_m)_o} \right) - \left(\frac{1}{(\rho_m)_i} \right) \right\} \quad (40)$$

For single-phase flows, this component is negligible, but can be significant in two-phase flows. For two-phase flow, the above equation can be used with ρ_m given by:

$$\frac{1}{\rho_m} = \left(\frac{x^2}{\rho_G \alpha} + \frac{(1-x)^2}{\rho_L (1-\alpha)} \right) \quad (41)$$

To evaluate the acceleration pressure drop due to density change, accurate prediction of the density of fluid is necessary.

Natural circulation is characterised by low mass flux since the driving head is less. To reduce pressure drop normally large diameter pipes are used. It is necessary to examine the validity of existing correlations at low mass flux and for flow through large diameter pipes.

3. HEAT TRANSFER IN SOURCE

3.1. Film heat transfer coefficient

Heat transfer coefficient, h, is normally expressed in terms of Nusselt Number (Nu), a dimensionless heat transfer parameter where Nu = hd / k. Relationships to determine h for flow through a pipe are discussed below.

3.1.1. Single phase laminar Flow

For constant wall temperature, the local Nusselt Number reaches a value of 3.65 asymptotically and for constant heat flux boundary condition, the local Nusselt number reaches a value of 4.36 asymptotically [33]. Hence, for developed flow through pipe, Nu of 3.65 for constant wall temperature and Nu of 4.36 for constant heat flux are recommended.

3.1.2. Single phase turbulent flow

The Dittus Boelter equation [34] given below is probably the most widely used correlation.

$$Nu = 0.023 \ Re^{0.8} Pr^{0.4} \quad (42)$$

Here the physical properties in the dimensionless numbers are evaluated at the bulk temperature of the fluid. For large temperature drop across the film the physical property most affected is the viscosity. The Sieder Tate equation [35] is frequently used in such cases.

$$Nu = 0.023 \ Re^{0.8} Pr^{0.4} . (\mu_w / \mu_b)^{0.14} \quad (43)$$

Here the physical properties are evaluated at fluid bulk temperature except for μ_w, which is evaluated at wall temperature.

3.1.3. Two phase flow

In two phase flow the vapor formed due to boiling and the liquid move together in a channel. It can be classified into subcooled flow and saturated flow. This classification refers to the temperature of the bulk of the liquid. In saturated two phase flow, the bulk of the liquid is at saturation temperature whereas in subcooled two phase flow, the bulk of the liquid is at lower temperature. However, in either case, to generate bubble the heated surface and adjacent layer of fluid are always at higher temperature than the saturation temperature. Heat transfer regions and flow regimes in a vertical diabatic channel are shown in Fig. 8 [36]. Correlations used to determine heat transfer coefficients in two phase flow are described below.

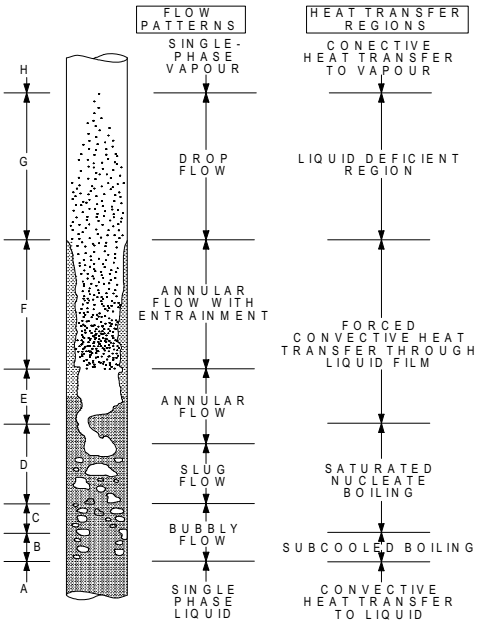

FIG.8. Regions of heat transfer in convective boiling.

Saturated Two Phase Flow Inside Horizontal and Vertical Tubes

Research in the flow boiling area has been directed towards gaining a fundamental understanding of the flow boiling phenomenon as well as towards obtaining experimental results that may be employed in equipment design, The fundamental studies clearly brought out the complexities of the flow boiling mechanisms (see Collier [36] for a comprehensive survey). Some of the major complexities involved are: bubble growth and departure behaviour in the flow field of a two-phase mixture, distribution of the two phases relative to each other and relative to the tube wall (flow pattern and entrainment effects), departure from thermodynamic equilibrium at local conditions, characteristics of the heat transfer surface, and the effect of fluid properties. There are a large number of saturated flow boiling correlations (well over 30) available in the literature. Two of them are described below.

a) *Kandlikar's Correlation [37]*

$$\frac{h_{TP}}{h_l} = C_1 Co^{C_2} (25 Fr_{LO})^{C_5} + C_3 Bo^{C_4} F_{fl} \tag{44}$$

$$C_O = \left(\frac{1-x}{x}\right)^{0.8} \left(\frac{\rho_G}{\rho_L}\right)^{0.5} \tag{45}$$

The values of constants C_1 to C_5 are given in Table 1. Co is the convection number, Bo the boiling number and h_l = single phase heat transfer coefficient with only the liquid fraction flowing in the tube. In the present work, the Dittus –Boelter equation is used to calculate h_l. Table-2 gives the values of the fluid-dependent parameters F_{fl}.

Table 1. Constants in the proposed correlation equation (44)

Constant	Convective region	Nucleate boiling region
C_1	1.1360	0.6683
C_2	-0.9	-0.2
C_3	667.2	1058.0
C_4	0.7	0.7
C_5*	0.3	0.3

*C_5=0 for vertical tubes, and for horizontal tubes with $Fr_{LO} > 0.04$

Table 2. Fluid dependent parameter F_{FL} in the proposed correlation, equation (44)

Fluid	F_{fl}
Water	1.00
R-11	1.30
R-12	1.50
R-1381	1.31
R-22	2.20
R-113	1.30
R-114	1.24
R-152a	1.10
Nitrogen	4.70
Neon	3.50

The two sets of values given in Table 1 correspond to the convective boiling and nucleate boiling regions, respectively. The heat transfer coefficient at any given condition is evaluated using the two sets of constants for the two regions, and since the transition from one region to another occurs at the intersection of the respective correlations, the higher of the two heat transfer coefficient values represents the predicted value from the proposed correlation.

b) Chen's Correlation [38]

This correlation includes both the heat transfer coefficients due to nucleate boiling as well as forced convective mechanisms.

$$h_{TP} = h_{mic} + h_{mac} \tag{46}$$

where h_{mic} is the nucleate boiling part and h_{mac} is the convective part

$$h_{mic} = h_{Foster\text{-}Zuber} . S \tag{47}$$

$$h_{mac} = h_{Dittus-Boelter} . F \tag{48}$$

where S & F are functions of Re_L and χ_{tt} respectively

S, suppression factor is the ratio of the effective superheat to wall superheat. It accounts for decreased boiling heat transfer because the effective superheat across the boundary layer is less than the super heat based on wall temperature.

$$S = \frac{1}{\left(1 + 2.53 \times 10^{-6}\ \mathrm{Re}_L^{1.17}\right)} \tag{49}$$

F, the enhancement factor is a function of the Martinelli Parameter χ_{tt}

$$F = 1 \quad \text{for} \frac{1}{\chi_{tt}} \le 0.1 \tag{50}$$

$$F = 2.35\left(\frac{1}{\chi_{tt}} + 0.213\right)^{0.736} \quad \text{for} \frac{1}{\chi_{tt}} > 0.1 \tag{51}$$

Forster – Zuber Correlation [39]

$$h = 0.0012 \left\{ \frac{k_L^{0.79} C_{pL}^{0.045} \rho_L^{0.49} g^{0.25}}{\sigma^{0.5} \mu_L^{0.29} h_{LG}^{0.24} \rho_G^{0.24}} \right\} \Delta T_W^{0.24} \Delta p^{0.75} \tag{52}$$

where $\Delta T = T_W - T_{sat}$

$\Delta p = P_{\text{wall temperature}} - P$

Subcooled flow

Chen's correlation [40] may be used for subcooled boiling.

$$h_{sub} = h_{mac} + h_{mic} \tag{53}$$

where, $h_{mac} = h_{\text{dittus-boelter}}$ (54)

$$h_{mic} = h_{\text{forster-zuber}} . S \tag{55}$$

h_{mac} is calculated using equation 43.

S can be calculated by using single phase Reynolds number with x=0 (using eqn. 49). For calculating $h_{\text{forster-zuber}}$ equation 52 is used.

Another correlation by Jens and Lottes [41] is also used widely.

$$h = \left[\frac{1}{25} \exp^{P/62}\right] \left(\Delta T_{sat}\right)^3$$

3.2. Critical heat flux (CHF)

Boiling crisis occurs when the heat flux is raised to such a high level that the heated surface can no longer support continuous liquid contact. This heat flux is usually referred to as the critical heat flux (CHF). It is characterized either by a sudden rise in surface temperature caused by blanketing of the

heated surface by a stable vapour layer, or by small surface temperature spikes corresponding to the appearance and disappearance of dry patches. Failure of the heated surface may occur once the CHF is exceeded.

In flow boiling the CHF mechanisms depend on the flow regimes and phase distributions, which in turn are controlled by pressure, mass flux and quality. For reactor conditions of interest, the flow quality generally has the strongest effect on CHF: the CHF decreases rapidly with an increase in quality. The following sections describe some important CHF mechanisms encountered at different qualities and flow conditions [4].

3.2.1. DNB (departure from nucleate boiling)

In subcooled and saturated nucleate boiling (approximate quality range: from –5% to +5%) the number of bubbles generated depends on the heat flux and bulk temperature. The bubble population density near the heated surface increases with increasing heat flux and a so-called bubble boundary layer often forms. If this layer is sufficiently thick it can impede the flow of coolant to the heated surface. This in turn leads to a further increase in bubble population until the wall becomes so hot that a vapour patch forms over the heated surface. This type of boiling crisis is also characterized by a fast rise of the heated surface temperature.

3.2.2. Dryout

In the annular dispersed flow regime (high void fraction) the liquid will be in the form of a liquid film covering the walls and entrained droplets moving at a higher velocity in the core. Continuous thinning of the liquid film will take place due to the combined effect of entrainment and evaporation. Near the dryout location the liquid film becomes very thin and due to the lack of roll waves (which normally occur at higher liquid film flow rates) entrainment is suppressed. If the net droplet deposition rate does not balance the evaporation rate the liquid film must break down. The temperature rise accompanying this film breakdown is usually moderate.

3.2.3. CHF Prediction Methodology

The complexity of predicting the CHF in a nuclear fuel bundle may be best understood by first considering the prediction of CHF of a simplest experimental setup; a uniformly heated tube cooled internally by a fluid flowing at a steady rate vertically upwards. Here the CHF is a function of the following independent variables:

$$CHF = f(De, G, \Delta H_{in}; P, E) \tag{57}$$

where E takes into account the effect of the heated surface, i.e. surface roughness, thermal conductivity and wall thickness.

Despite the simplicity of the experimental setup, over 400 correlations for CHF in tubes are currently in existence. The present proliferation of correlations illustrates the complex state-of-the-art in predicting the CHF phenomenon even for simple geometry at steady-state flow conditions.

Analytical models

Analytical CHF models are based on physical mechanisms. The most common models that have met with some success are

a) Annular film dryout model [42]
b) Bubbly layer model [43]
c) Helmholtz instability model [44]

However, because of our limited understanding of the mechanisms involved, the models are still less accurate than empirical correlations.

Empirical methods

INLET-CONDITIONS-TYPE PREDICTION METHODS

For a given geometry and inlet conditions, the critical power N_{DO} i.e. power corresponding to the first occurrence of CHF for that geometry is expressed as

$$N_{DO} = f(P_{in}, G_{in}, T_{in,} \text{ c/s}, L_H) \quad (58)$$

This method cannot be used for predicting the location and magnitude of CHF

LOCAL-CONDITIONS –TYPE PREDICTION METHODS

This type of prediction methods follow the local-conditions hypothesis which states that the local CHF is dependent only on the local conditions and not on upstream history.

$$CHF = f(P,G,X_{DO}, \text{c/s}) \quad (59)$$

The local conditions approach, is probably the most common method for predicting CHF. This form is more convenient since it depends on fewer parameters and permits the prediction of the location of CHF.

The large majority of the CHF prediction methods proposed are of this type. It is conservatively estimated that there are over 400 empirical correlations of this type proposed in the literature for directly heated tubes. Their main disadvantage is their limited range of application.

CHF LOOK-UP TABLE METHOD

The CHF look up table is basically a normalized data bank. The recently completed International CHF look up table [45] provides CHF values for water cooled tubes, at discrete values of pressure (P), mass flux (G), and quality (X), covering the ranges of 0.1 – 21 Mpa pressure, 0-8000 $kg.m^{-2}.s^{-1}$ (zero flow refers to pool-boiling conditions) mass flux and –50% to 100% vapour quality (negative qualities refer to subcooled conditions). Linear interpolation between table values is used for determining CHF. Extrapolation is usually not needed as the table covers a range of conditions much wider than any other prediction method. Groeneveld et al. [45] have presented a complete description of the Look up table for tubes. As an example, the 2005 CHF look up table for critical heat flux in 8mm tubes for 7.0 MPa is reproduced in Table 3.

The look up table needs to be converted into a prediction method for bundle geometries for nuclear reactor application. The CHF needs to be modified to account for bundle specific effects. The following correction factor methodology is adopted to evaluate the bundle CHF:

$$CHF_{bundle} = CHF_{table} \times K_1 \times K_2 \times K_3 \times K_4 \times K_5 \times K_6 \times K_7 \times K_8 \quad (60)$$

where CHF_{bundle} is cross section average value of the heat flux at which the CHF first occurs at the cross-section, CHF_{table} is the CHF value for a tube as found in the look up table for the same cross-sectional average values of P and G, and K_1 to K_8 are correction factors to account for specific bundle effects. A summary of correction factors is given in Table 4.

Table 3. The 2005 CHF Look-up table for critical heat flux in 8 MM tubes (in kW/M^2)

Pressure kPa	Mass Flux $kg/m^2 s$	Quality																						
		-0.50	-0.40	-0.30	-0.20	-0.15	-0.10	-0.05	0.00	0.05	0.10	0.15	0.20	0.25	0.30	0.35	0.40	0.45	0.50	0.60	0.70	0.80	0.90	1
7000	0	5445	5059	4676	4323	4139	3937	3677	3322	2696	2256	1848	1479	1243	1036	891	778	692	621	525	389	267	209	0
7000	50	5919	5536	5191	4863	4698	4520	4306	3998	3399	2986	2624	2264	2042	1859	1712	1588	1477	1366	1151	1010	473	325	0
7000	100	6912	6301	5871	5584	5462	5261	5095	4849	4271	3776	3499	3290	3142	3034	2906	2850	2651	2486	2123	1673	1205	768	0
7000	300	7445	6709	6259	6020	5914	5761	5662	5495	5182	4752	4464	4070	3764	3611	3417	3250	3028	2738	2286	1994	1408	869	0
7000	500	7842	6895	6435	6188	5996	5931	5818	5672	5408	4922	4521	4196	3989	3812	3602	3459	3221	2905	2482	1985	1547	869	0
7000	750	9129	7841	6867	6263	6154	5998	5895	5776	5430	4987	4538	4131	3918	3709	3464	3327	3118	2770	2312	1904	1400	742	0
7000	1000	10186	8774	7390	6532	6313	6276	6162	5864	5366	4920	4399	3935	3723	3447	3112	2884	2713	2432	2085	767	506	341	0
7000	1500	11920	10072	8460	7262	6915	6647	6308	5729	5059	4561	4039	3612	3279	2991	2698	2490	2264	1591	599	372	318	191	0
7000	2000	13294	11209	9172	7557	7279	6769	6187	5327	4570	4020	3552	3174	2864	2566	2353	1919	1406	793	483	267	197	134	0
7000	2500	14680	12245	9774	7920	7382	6765	5895	4977	4178	3639	3207	2867	2552	2211	1941	1487	813	521	342	177	103	58	0
7000	3000	15871	13214	10463	8259	7522	6778	5785	4761	3971	3366	3014	2640	2333	2111	1685	951	493	429	307	157	77	43	0
7000	3500	16889	14072	11223	8783	7744	6972	5738	4518	3739	3127	2816	2482	2188	1798	1357	851	631	531	388	224	96	44	0
7000	4000	17783	14824	11868	9277	8077	7118	5593	4226	3539	2855	2616	2362	2104	1710	1251	957	789	681	444	255	99	44	0
7000	4500	18619	15498	12439	9619	8281	7208	5381	4156	3422	2650	2472	2268	2057	1647	1239	1006	867	779	487	266	102	45	0
7000	5000	19434	16132	12870	10084	8686	7415	5486	4350	3409	2611	2486	2251	2040	1619	1279	1052	950	854	526	277	106	47	0
7000	5500	20138	16733	13579	10563	9272	7844	6153	4649	3405	2688	2460	2325	2076	1662	1397	1217	1065	933	576	298	115	52	0
7000	6000	20703	17309	14047	11354	9947	8657	6697	4756	3417	2725	2487	2353	2087	1697	1476	1339	1184	1018	637	327	131	60	0
7000	6500	21284	17855	14610	11951	10355	9156	7135	4905	3437	2733	2525	2442	2241	1938	1688	1515	1303	1103	702	360	149	69	0
7000	7000	21889	18357	15013	12260	10817	9456	7309	4949	3504	2872	2648	2499	2348	2094	1852	1615	1393	1182	771	401	170	80	0
7000	7500	22505	18841	15385	12539	11244	9779	7455	5004	3629	3017	2792	2596	2488	2263	2039	1776	1504	1264	838	433	182	86	0
7000	8000	23064	19305	15794	12917	11519	10059	7792	5163	3777	3222	3120	3063	2927	2605	2282	1893	1592	1345	904	463	193	91	0

Table 4. Summary of correction factors applicable to the CHF look-up table [4]

FACTOR	FORM	COMMENTS
K_1 Sub channel or Tube Diameter Cross- Section Geometry Factor	For $2 \le D_{hy} \le 25\,mm$: $K_1 = (0.008/D_{hy})^{1/2}$ For $D_{hy} > 25\,mm$ $K_1 = 0.57$	Includes the observed diameter effect on CHF. This effect is slightly quality dependent.
K_2, Bundle-Geometry Factor	$K_2 = \min[1, (0.5 + 2\delta/d)\exp(-0.5x^{1/3})]$	This is a tentative expression, an empirically derived factor is preferred. K_2 is also a weak function of P, G and X.
K_3, Mid-Plane Spacer Factor for a 37- element Bundle	$K_3 = 1 + A\exp(-B L_{sp}/D_{hy})$ $A = 1.5 K_L^{0.5} (G/1000)^{0.2}$ $B = 0.1$	This factor has been validated over a limited range of spacer geometries.
K_4, Heated - Length Factor	For $L/D_{hy} \ge 5$: $K_4 = \exp[(D_{hy}/L)\exp(2\alpha_h)]$ $\alpha_h = X\rho_L/[X\rho_L + (1-X)\rho_G]$	Inclusion of α_h correctly predicts the diminishing length effect at subcooled conditions.
K_5, Axial Flux Distribution Factor	For $X \le 0: K_5 = 1.0$ For $X > 0: K_5 = q_{loc}/q_{BLA}$	Tong's F-factor method [46] May also be used within narrow ranges of conditions.
K_6, Radial or Circumferential Flux Distribution Factor	For $X > 0: K_6 = q(z)_{avg}/q(z)_{max}$ For $X \le 0: K_6 = 1.0$	Tentative recommendation only and to be used with well-balanced bundle. May be used for estimating the effect of flux tilts across elements. Otherwise method of Yin (1991) [47] is recommended.
K_7, Flow- Orientation Factor	$K_7 = 1 - \exp(-(T_1/3)^{0.5})$ where $T1 = \left(\frac{1-X}{1-\alpha}\right)^2 \frac{f_L G^2}{g D_{hy} \rho_L (\rho_L - \rho_G)\alpha^{0.5}}$ f_L is the friction factor of the channel.	This equation was developed by Wong and Groeneveld [48] based on the balance of turbulent and gravitational forces. The void fraction is evaluated with the correlation of Premoli et al. [49].
K_8, Vertical Low- Flow Factor	$G < -400\,kg\,m^2\,s^{-1}$ or $X << 0$: $K_8 = 1$ $-400 < G < 0\,kg\,m^2\,s^{-1}$: Use linear interpolation between table value for upward flow and value predicted form $CHF = CHF_{G=0,X=0}(1-\alpha_{hom})C_1$	For $\alpha_h < 0.8$: $C1 = 1.0$ For $\alpha_{hom} \ge 0.8$: $C_1 = \frac{0.8 + 0.2\rho_L/\rho_G}{\alpha_{hom} + (1-\alpha_{hom})\rho_L/\rho_G}$ Minus sign refers to downward flow. G=0, X=0 refers to pool boiling.

4. HEAT TRANSFER IN SINK

4.1. Boiling

As stated earlier, boiling takes place on the secondary side of steam generators. To determine heat transfer coefficients on the secondary side of steam generators , the correlations given in section 3 can be used.

4.2. Condensation

Condensation occurs when the temperature of vapor is reduced below its saturation temperature T_{sat}. Vapor starts condensing on the surface when the surface is cooled below the saturation temperature of vapor. Two distinct forms of condensation on the surface are observed; Film condensation and Dropwise condensation as shown in Fig 9.

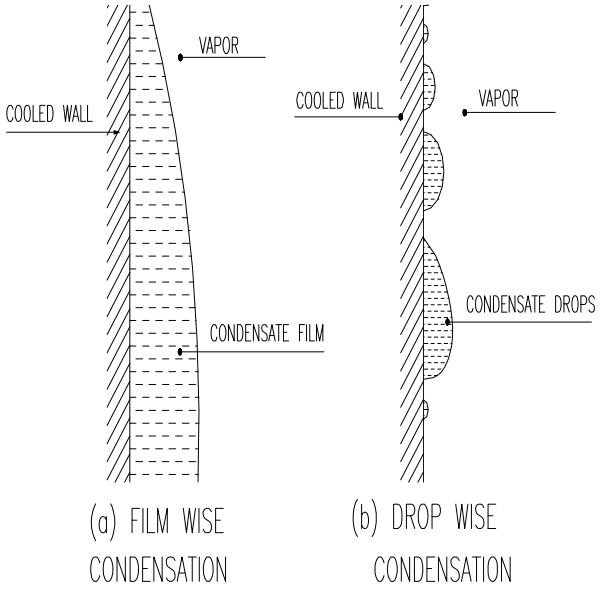

FIG. 9. Filmwise and dropwise condensation.

In film condensation the condensate wets the surface and forms a liquid film on the surface while in dropwise condensation the condensed vapor forms droplets on the surface instead of a continuous film and the surface is covered by countless droplets of varying diameters.

In film condensation the surface is blanketed by a liquid film of increasing thickness and this "liquid wall" between solid surface and the vapor serves as a resistance to heat transfer. The heat of vaporization h_{fg} released, as the vapor condenses, must pass through this resistance before it can reach the solid surface and be transferred to the medium on the other side. In dropwise condensation part of the surface is in contact with vapor leading to higher heat transfer rates.

Flow regimes in condensation heat transfer

The Reynolds number ($\mathrm{Re} = \frac{4\dot{m}}{p\mu_L}$) for condensation on the outer surfaces of vertical tubes or plates increases in the flow direction due to the increase of the liquid film thickness δ. The flow of liquid film exhibits different regimes depending on the value of the Reynolds number. It is observed that outer surface of the liquid film remains smooth and wave-free for about Re<30 and thus the flow is clearly

laminar. Ripples or waves appear on the free surface of the condensate flow as the Reynolds number increases, and the condensate flow becomes fully turbulent at about Re≈1800.The condensate flow is called wavy-laminar in the range 30<Re<1800 and turbulent for Re>1800. However, some disagreement exists about the value of Re at which the flow becomes wavy-laminar or turbulent.

4.2.1. Vertical plates

Laminar Flow on a smooth vertical plate

The analytical relation for the heat transfer coefficient in the laminar film condensate on vertical plate was first developed by Nusselt [50]. The average heat transfer coefficient over the entire vertical plate is determined as follows

$$h = h_{ave} = \frac{1}{L}\int_0^L h_x dx = \frac{4}{3}h_{x=L} = 0.943\left[\frac{g\rho_L(\rho_L - \rho_G)h_{fg}k_L^3}{\mu_L(T_{sat} - T_w)L}\right]^{\frac{1}{4}} \quad (61)$$

Where, x= distance from leading edge and L=length of the plate

This equation under predicts heat transfer because it does not take into account the effects of the nonlinear temperature profile in the liquid film and cooling of the liquid below the saturation temperature. Both of these effects can be accounted for by replacing h_{fg} with h_{fg}^* given by equation (62).

$$h_{fg}^* = h_{fg} + 0.68C_{pL}(T_{sat} - T_w) \quad (62)$$

The modified latent heat of vaporization h_{fg}^* is used to consider the extra heat that is released when the condensate in the actual condensation process is cooled further to some average temperature between T_{sat} and T_w. In equation (61) h_{fg} is substituted by h_{fg}^*.

Wavy Laminar Flow on Vertical Plates

At Reynolds numbers greater than about 30, it is observed that waves form at the liquid-vapor interface although the flow in liquid remains laminar. The flow in this case is said to be wavy laminar. The waves at the liquid-vapor interface tend to increase heat transfer. But the waves also complicate the analysis and make it very difficult to obtain analytical solutions. Therefore, we have to rely on the experimental studies. The increase in heat transfer due to wave effect is on the average about 20 percent but it can exceed 50 percent.

Kutateladze [51] recommended the following relation, based on his experimental studies, for the average heat transfer coefficient in wavy laminar condensate flow for $\rho_G \langle\langle \rho_L$ and 30<Re<1800,

$$h_{vert,wavy} = \frac{Rek_L}{1.08Re^{1.22} - 5.2}\left(\frac{g}{\nu_L^2}\right)^{1/3} \quad (63)$$

A simpler alternative to the relation above proposed by Kutateladze [51] is

$$h_{vert,wavy} = 0.8Re^{0.11}h_{vert(smooth)} \quad (64)$$

Turbulent Flow on Vertical Plates

At a Reynolds number of about 1800, the condensate flow becomes turbulent. Several empirical relations of varying degrees of complexity are proposed for the heat transfer coefficient for turbulent flow. The Re relation in this case is given by

$$\mathrm{Re} = \frac{4Q_{conden}}{p\mu_L h_{fg}^*} = \frac{4Ah(T_{sat} - T_w)}{p\mu_L h_{fg}^*} \tag{65}$$

Labuntsov [52] proposed the following relation for the turbulent flow of the condensate on vertical plates:

$$h_{vert,turbulent} = \left(\frac{\mathrm{Rek}_L}{8750 + 58\mathrm{Pr}^{-0.5}\left(\mathrm{Re}^{0.75} - 253\right)} \left(\frac{g}{\nu_L^2} \right)^{\frac{1}{3}} \right) \quad , \qquad \mathrm{Re}>1800,\ \rho G << \rho_L \tag{66}$$

The physical properties of the condensate are to be evaluated at the film temperature $T_f = (T_{sat} + T_w)/2$.

For vertical tubes, the above equations for vertical plate can be used with height of tube as characteristic length.

4.2.2. Horizontal tubes and spheres

Nusselt's analysis of film condensation on the vertical plates can also be extended to horizontal tubes and spheres .The average heat transfer coefficient for film condensation on the outer surfaces of a horizontal tube is determined to be

$$h_{horiz} = 0.729 \left[\frac{g\rho_L(\rho_L - \rho_G)h_{fg}^* k_L^3}{\mu_L (T_{sat} - T_W) D} \right]^{1/4} \tag{67}$$

This relation can be modified for the sphere by replacing the constant 0.729 by 0.815.

A comparison of the heat transfer coefficient relations for a vertical tube of height L and a horizontal tube of diameter D yields

$$\frac{h_{vert}}{h_{horiz}} = 1.29 \left(\frac{D}{L} \right)^{1/4} \tag{68}$$

Setting $h_{vert} = h_{horiz}$ gives $L = 1.29^4 D = 2.77D$, which implies that for a tube whose length is 2.77 times its diameter, the average heat transfer coefficient for laminar film condensation will be the same whether the tube is positioned horizontally or vertically. For L>2.77D, the heat transfer coefficient will be higher in a horizontal position. Considering that the length of a tube in any practical application is several times its diameter, it is common practice to place the tubes in a condenser horizontally to maximize the condensation heat transfer coefficient on the outer surfaces of the tubes.

4.2.3. Horizontal tube banks

Horizontal tubes stacked on top of each other are commonly used in condenser design. The average thickness of the liquid film at the lower tubes is much larger as a result of condensate falling on top of them from the tubes directly above. Hence the average heat transfer coefficient at the lower tubes in such arrangements is smaller. Assuming the condensate from the tubes drain smoothly to the tubes

below it, the average film condensation heat transfer coefficient for all the tubes in a vertical tier can be expressed as [53]

$$h_{horiz,Ntubes} = 0.729\left[\frac{g\rho_L(\rho_L-\rho_G)h_{fg}^{*}k_L^3}{\mu_L(T_{sat}-T_w)ND}\right]^{1/4} = \frac{1}{N^{1/4}}h_{horiz,1tube} \tag{69}$$

where, N = No. of tubes

This relation doesn't take into account the increase in heat transfer due to the ripple formation and turbulence caused during drainage and thus generally yields conservative results.

4.2.4. Condensation inside horizontal tubes

So far we have discussed film condensation on the outer surfaces of tubes and other geometries which is characterized by negligible vapor velocity and unrestricted flow of the condensate. Heat transfer analysis of condensation inside tubes is complicated by the fact that it is strongly influenced by vapor velocity and the rate of liquid accumulation on the walls of the tubes.

For low vapor velocities Chato [54] recommends the following expression for condensation

$$h_{internal} = 0.555\left[\frac{g\rho_L(\rho_L-\rho_G)k_L^3}{\mu_L(T_{sat}-T_w)}\left(h_{fg}+\frac{3}{8}C_{pL}(T_{sat}-T_w)\right)\right]^{1/4} \tag{70}$$

for

$$Re_G = \left(\frac{\rho_G V_G D}{\mu_G}\right)_{inlet} < 35{,}000 \tag{71}$$

where, Reynolds number for vapor is to be evaluated at the tube inlet conditions using the internal tube diameter as the characteristic length. T_L is the liquid temperature and is average of the wall and saturated steam temperatures.

4.2.5. Effect of the presence of noncondensable gases

In nuclear reactors, the condensation of steam in presence of noncondensable gas becomes an important phenomenon when steam released from the core mixes with the containment air following a Loss of Coolant Accident. Steam condenses in presence of noncondensable gas when flowing inside the vertical tubes of passive containment coolers. The drastic reduction in the condensation heat transfer coefficient in the presence of noncondensable gas can be explained as follows: When the vapor mixed with a noncondensable gas condenses, the noncondensable gas remains in the vicinity of the condensate layer. This gas acts as a barrier between the vapor and the condensate layer as shown in Fig. 10 and makes it difficult for the vapor to reach the surface. The vapor now must diffuse through the noncondensable gas first before reaching the surface and this reduces the effectiveness of the condensation process. Most condensers used in power plants operate at pressure below the atmospheric pressure and operation at such a low pressure raises the possibility of air leaking into the condensers. Variation of heat transfer coefficient with non-condensable mass fraction is shown in Fig. 11 [55].

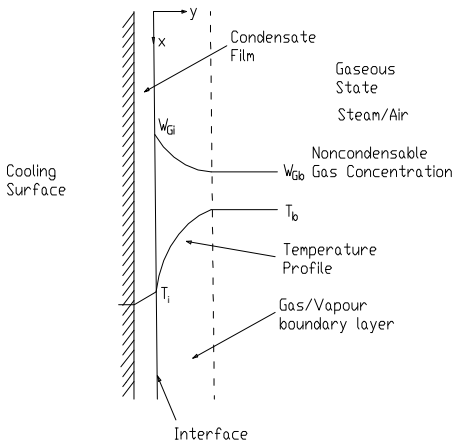

FIG.10. Condensation in presence of non-condensables

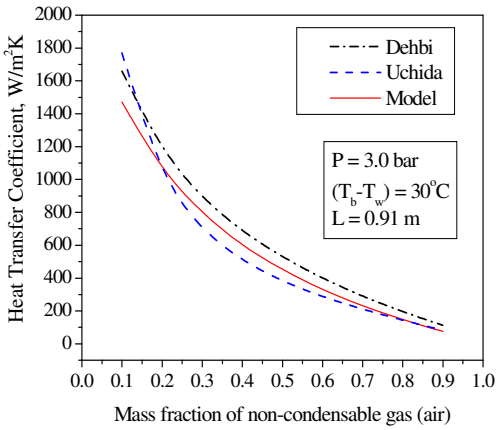

FIG.11. Heat transfer coefficient vs. mass fraction

Condensation when steam/noncondensable mixture is non-flowing:

There are number of correlations available in the literature. Some of the correlations developed are given below.

The correlation developed by Uchida [56]

$$h_{Uchida} = 380\left(\frac{W_{nc}}{1-W_{nc}}\right)^{-0.7} \tag{72}$$

where, W_{nc} is the noncondensable mass fraction in the steam/noncondensable mixture. Experiments performed by Uchida were in fixed volumes with constant inventories of non-condensable gas (at atmospheric pressure). Wall temperature was held constant.

The Dehbi correlation [57]

$$h_{Dehbi} = \frac{L^{0.05}\left[(3.7+28.7P_{tot})-(2438+458.3P_{tot})\log W_{nc}\right]}{(T_b-T_w)^{0.25}} \tag{73}$$

This correlation is applicable for the following conditions

0.3 m < L < 3.5 m
1.5 atm. < P_{tot} < 4.5 atm.
10 °C < (T_b-T_w) < 50 °C

Condensation when steam / noncondensable gas flowing inside vertical tube:

For the calculation of condensation heat transfer coefficient, h_c, the correlation developed by Siddique [58] is given as

$$Nu(x) = 1.137 Re_G^{0.404} W_a^{-1.105} Ja^{-0.741} \tag{74}$$

which applies in the following range of experiments

$$0.1 < W_a < 0.95$$
$$445 < Re_G < 22700$$
$$0.004 < Ja < 0.07$$

W_a is the air mass fraction in the steam/air mixture. The Jakob number, Ja, C_{pG} $(T_b-T_{wi})/h_{fg}$, is defined as the ratio of the sensible energy transfer in the vapor to phase change energy.

5. OTHER RELEVANT PHENOMENA

Aksan et. al. [61] have provided an extensive list of important thermal hydraulic phenomena for advanced reactor designs. Out of these, phenomena relevant for natural circulation are included in this section.

5.1. Thermal Stratification

Thermal stratification as the name suggests, denotes formation of horizontal layers of fluid of varying temperature with the warmer layers of fluid placed above the cooler ones. Thermal stratification is encountered in large pool of water increasingly being used as heat sink in new generation of advanced reactors. These large pools (capacity up to several thousand cubic meters) at near atmospheric pressure provide a heat sink for hest removal from the reactor or the containment by natural circulation as well as a source of water for core cooling. Examples include the pressure suppression pool of the ESBWR, the in-containment refueling water storage tank of the AP-1000, the gravity driven water pool of AHWR. Stratification influences heat transfer to pool to a great extent and heat storage capacity of the pool in the form of sensible heat is significantly reduced.

When a heat source is placed vertically in a pool of water, the fluid adjacent to the source gets heated up. In the process, its density reduces and by virtue of the buoyancy force, the fluid in this region moves up. After reaching the top free surface, the heated water takes a turn, moves towards the wall of the pool along the surface. Since, density of this heated water is low, it does not flow downward. If a vertical sink is provided, downward flow takes place in a narrow region adjacent to the sink. Over a period of time, depending on the size and geometry of the pool and the source, the greater part of the pool gets thermally stratified except the regions close to the heat source and the heat sink. In the region of the thermal stratification fluid is almost static.

The forces involved in the flow field described above are buoyancy force, viscous force and inertia force. In many cases, one has to consider turbulence. In case of free surface, mass transfer and heat transfer are to be considered at the free surface.

Towards the understanding of the complex flow pattern in a pool, one of the commonly followed approaches is the study of natural convection in heated enclosures. The enclosures are either differentially heated (with one wall heated and the other wall cooled) or symmetrically heated (both the walls equally heated while heat dissipation to atmosphere is allowed at the top). The bottom and top walls are kept adiabatic in the former case while only the bottom wall is maintained adiabatic in the latter case. The studies have indicated the importance of few parameters governing the flow phenomenon like Rayleigh number, Prandtl number and the aspect ratio of the enclosure (the ratio of height to the width of the enclosure). Depending on the magnitude of the Rayleigh number, the flow can be laminar or turbulent. Using finite volume techniques, transient CFD models are being developed for several of these cases for the prediction of flow patterns and temperature profiles. In particular, the stress is on developing better turbulence models, which require optimum computational effort and are satisfactorily accurate. For validation of theoretical results, experimental data are being generated. A typical velocity profile in a side heated enclosure is shown in Fig. 12. From this figure, it may be noted that close to the top surface a narrow horizontal loop is formed [59,60]. Fig. 13 depicts temperature distribution in a pool following heat transfer from an immersed isolation condenser obtained using a CFD code. Nucleate boiling at the outer surface of IC tubes is often encountered. The heat sources in the pool need not be of equal strength and are not homogeneously distributed. Suitable analytical models are being developed to address these issues.

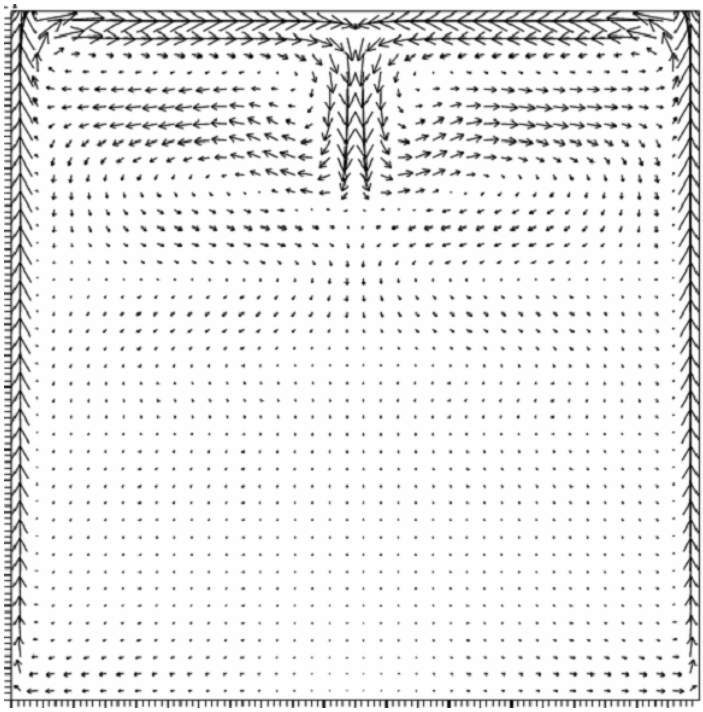

FIG. 12. Velocity plots.

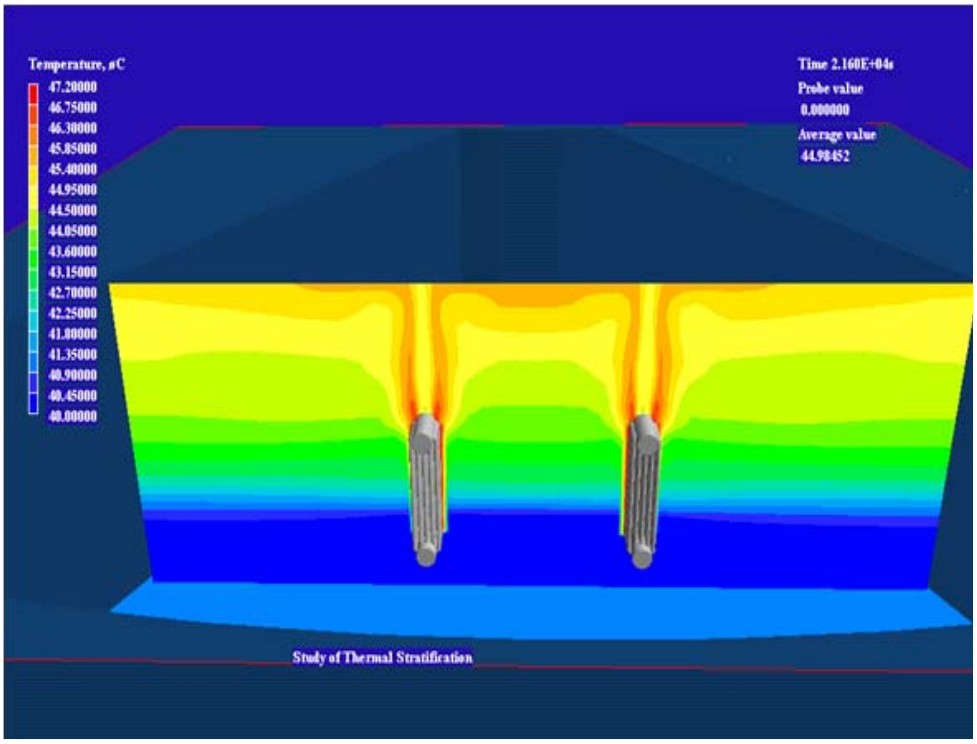

FIG. 13. Temperature distribution in IC pool

5.2. Carryover

Water in the form of droplets may get carried over with steam to the turbine, which can be detrimental to turbine because of erosion of turbine blades. Two-phase mixture leaving the core of the reactor enters the steam drum through risers (Fig. 14). Normally steam–water separation is effected in steam drum or stream generator using suitably designed mechanical separators. Since, pressure drop across mechanical separators is quite large, in natural circulation systems steam – water separation is normally effected by gravity without using mechanical separators. This may result in liquid carryover with the steam to the turbine. Carryover to the turbine is to be restricted to a permissible maximum value of about 0.2%, by incorporating appropriate measures at the design stage, and hence, should be predicted accurately under different operating conditions.

Droplet carryover is a phenomenon associated with droplet entrainment, which is an outcome of dynamic interaction of two phases in relative motion. Various researchers have studied entrainment and two categories of entrainment are identified as film entrainment and pool entrainment. Film entrainment is entrainment of droplets from the liquid film by various mechanisms like roll wave shear-off and is typified by presence of a wavy interface of liquid film and vapor, broadly along the direction of flow. Dispersed annular flow is the typical flow regime exemplifying the film entrainment. On the other hand, pool entrainment is entrainment of droplets from the surface of pool due to bursting of bubbles and break-up of liquid jet. Pool entrainment is typified by the presence of liquid pool and turbulent liquid vapor flow. Modeling the entrainment requires the appropriate droplet formation mechanism, and prediction of average or maximum droplet size distribution function.

Film entrainment models and pool entrainment models are used to determine carryover. Zuber [62] studied entrainment associated with droplet formation due to bursting of bubbles on the surface of liquid pool and break-up of liquid jets. Ishii and Kataoka [63] have proposed the entrainment at the surface of pool as a function of physical properties. Entrainment is found to be a function of steam velocity and height from the free surface.

5.3. Carryunder

Carryunder is the entrainment of gas bubbles with the recirculating liquid (Fig. 14). Carryunder is particularly undesirable in a natural circulation system due to impaired thermal-margin, since the driving potential for the flow is density difference between hot and cold legs.

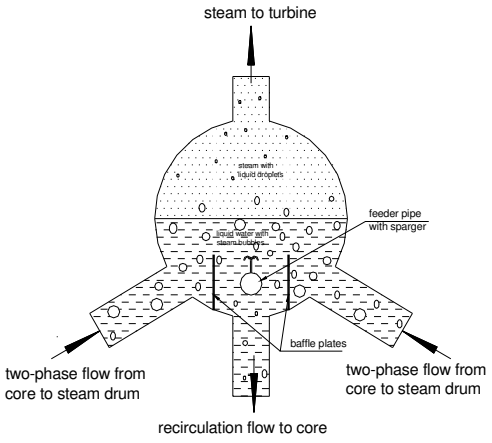

FIG. 14. Schematic of steam drum depicting carryover & carryunder.

Carryunder depends on bubble dynamics as well as the geometrical configuration of flow path. Bubble dynamics is governed by various forces acting on the moving bubbles, of which the drag force is most significant and most uncertain to predict because of uncertainties in drag coefficient. Various researchers have empirically obtained the drag coefficient for various flow regimes. Geometrical

parameters affecting the entrainment are the baffle spacing and liquid level with respect to baffle tip. Increasing the baffle spacing first increase the Carryunder due to large inter-baffle space available for entrainment and then decrease due to very low liquid velocity in the inter-baffle space. Thus with regard to baffle space, Carryunder may be attributed to area dominated regime and velocity dominated regime.

5.4. Parallel channel effect

In respect of natural circulation, interaction between multiple parallel flow paths may become a critical phenomenon mainly in respect of instability. Presence of multiple parallel channels connected to two plenums and having different heat fluxes offer the possibility of number of flow configurations in which some channels may have flow direction opposite to others and some may even stagnate. Another important phenomenon related to parallel channel instability is the oscillation in one group of channels 180° out of phase with oscillation in another group. This phenomenon is of special concern since this instability may not be detectable by monitoring total flow in the loop.

5.5. Effect of non-condensable gases

Containment:

Containment is the final physical barrier to prevent release of radioactivity to environment. To maintain structural integrity of the containment it is necessary to remove energy released into the containment under accidental condition. Passive containment cooling is provided to condense steam released into the containment by following means: a) incorporation of Building Condensers as in SWR-1000 and AHWR (fig.15a), b) Isolation Condensers immersed in large water pools as in ESBWR (fig.5), c) external cooling of containment surface as in AP-1000 by natural convection of air and water spray (fig.15b). In this case condensation of steam takes place at the inner surface. The performance of these condensers are highly impaired by the presence of non-condensable gases.

Besides air present in the containment, depending on the severity of accident, hydrogen and fission gases may also get released into the containment. It is necessary to predict distribution of hydrogen, steam and air in the containment to assess the performance of the condensers. Potential stratification and separation of steam and non-condensable gases constitute an important factor for containment cooling. Many experiments have been conducted and various computer codes developed to predict the distribution of steam and non-condensable gases and the performance of condensers [64].

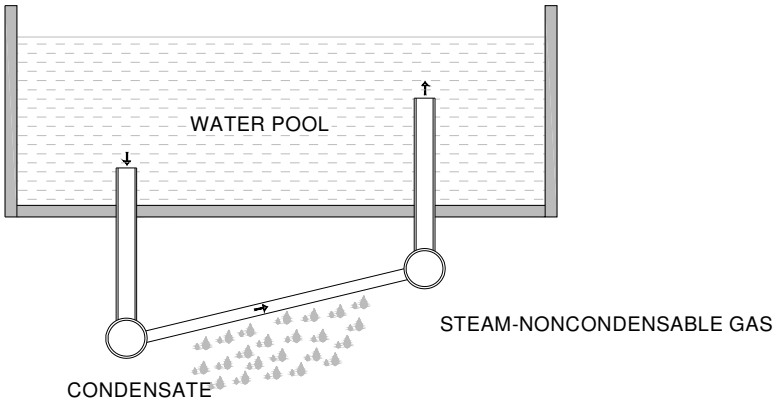

FIG. 15a Passive Containment Cooling System

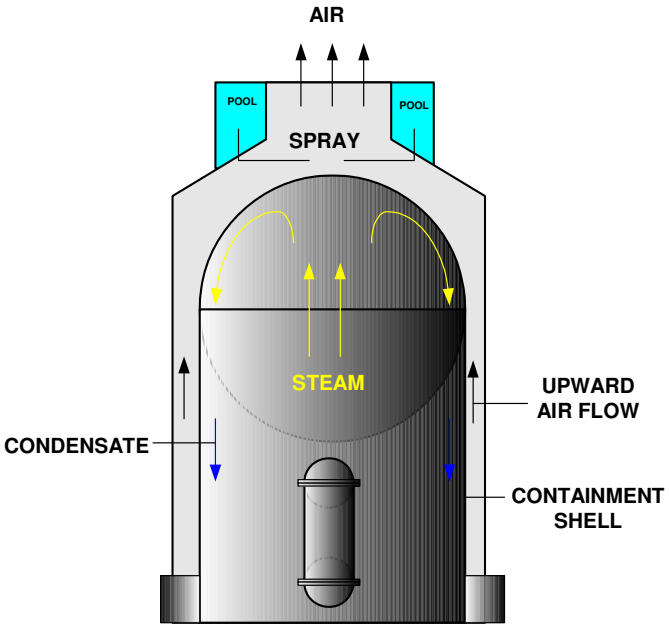

FIG.15b Passive cooling of containment surface

Primary Loop:

Non-condensable gases, if released into a loop may get accumulated at specific locations depending on the configuration and can inhibit natural circulation. For instance, in a PHWR non-condensable gases may accumulate at the U-bend at the top of the inverted U tubes of steam generators since the driving head is low under accidental conditions. This may reduce or completely stop flow through the tube.

5.6. Vortex formation in pool

As stated earlier, in many advanced reactor designs a large pool of water is provided which acts as a heat sink for many passive heat removal systems and/or source for low pressure injection of coolant into the core under accidental condition. Flow of water by gravity through small outlet pipes of these pools may lead to vortex formation [61]. Depending on the orientation of the outlet port and the depth of water above the port air or gas from top of pool may get entrained into the water. Presence of these non- condensable gases in cooling water will have adverse effect on core cooling.

5.7. Fluid mixing

Boric acid is introduced into the reactor coolant to control long term reactivity. Forced coolant circulation during normal operation ensures that the boric acid is homogeneously distributed in the reactor coolant system so that the boron concentration is practically uniform. Decrease of boron concentration in core results in an increase of reactivity. During a small break LOCA in a PWR the energy transport from core to the steam generators which depends on the primary coolant inventory is ensured by either single/two phase natural circulation or by reflux condenser mode of operation. The steam which is generated in core is largely devoid of boron so that the condensate formed in the SGs during reflux condenser mode is also largely un-borated. If reflux condensation is maintained for prolonged period, boron diluted condensate may accumulate in the loop seals (fig. 16). The restart of natural circulation after refilling of primary or restart of pumps can then lead to displacement of low boron concentration water from loop seal into the reactor vessel and possibly into the core which can result in re-criticality and power excursion. The effect of boron diluted water entering vessel on core behavior strongly depends on mixing of water with different boron concentrations in the cold legs, downcomer and the lower plenum region. In recent years, renewed focus has been placed on the study of these accident scenarios. More emphasis is placed on fluid mixing phenomena taking place during

boron dilution. Extensive experimental and theoretical studies have been conducted in this area [65,66,67]. Experiments have been conducted in the integral test facility, PKL and the Upper Plenum Test Facility (UPTF) in Germany in this area [68].

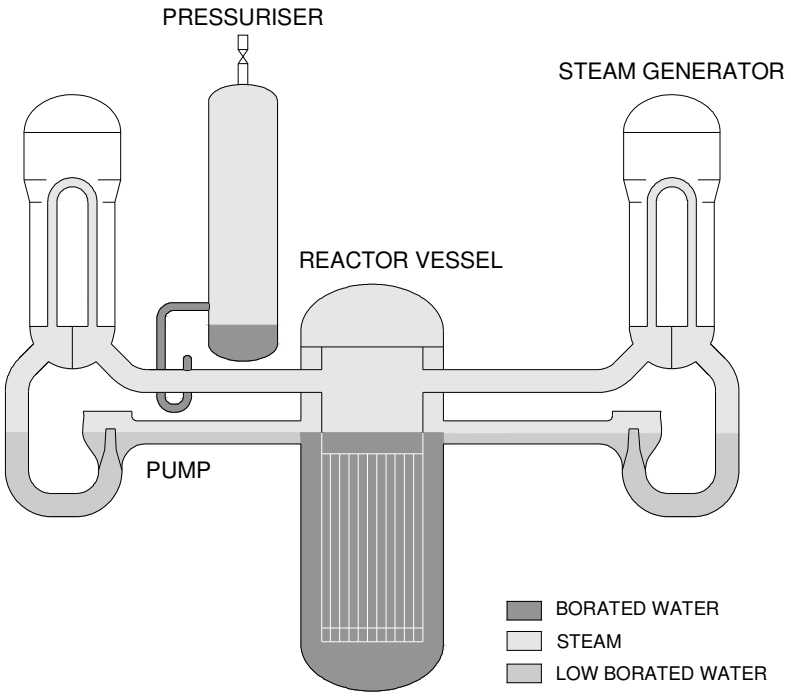

FIG. 16. Low Borated Water in Loop Seal

Under accidental condition coolant injected into the cold leg is normally much cooler than the water in the vessel. In absence of proper mixing, difference in fluid temperature may lead to unacceptable thermal gradient affecting structural integrity. CFD plays a very important role in the study of fluid mixing.

5.8. Counter-current flow limitation (CCFL)

The onset of flooding or countercurrent flow limitation (CCFL) determines the maximum rate at which one phase can flow counter currently to another phase. The thermal-hydraulic analysis of countercurrent two-phase flow has been of great importance in connection with the safety analysis of nuclear reactor systems. In the event of a loss of coolant accident (LOCA), steam is produced in the core of a pressurized water reactor (PWR). This steam flows upward through the hot leg, moving counter currently to the flow of injected emergency core cooling water (Fig. 17). Steam condensed in the steam generator also flows back to the core. The cooling water should be able to flow, past the upcoming steam, into the core. However, this emergency core cooling (ECC) is limited by the flooding phenomenon that partly or totally inhibits the water flow into the core. To evaluate the effectiveness of ECC it is necessary to study countercurrent flow of the phases. Somchai Wangwises [69] has carried out extensive work on two-phase countercurrent flow in a model of PWR hot leg. The CCFL has been studied by a large number of researchers, both experimentally and analytically, mostly in vertical pipes. The CCFL in horizontal or nearly horizontal geometries has received comparatively little attention in the literature. H.T. Kim [70] has studied CCFL in horizontal-to-inclined pipes simulating a PWR hot leg. The study revealed the effect of L/D of pipes on CCFL phenomena.

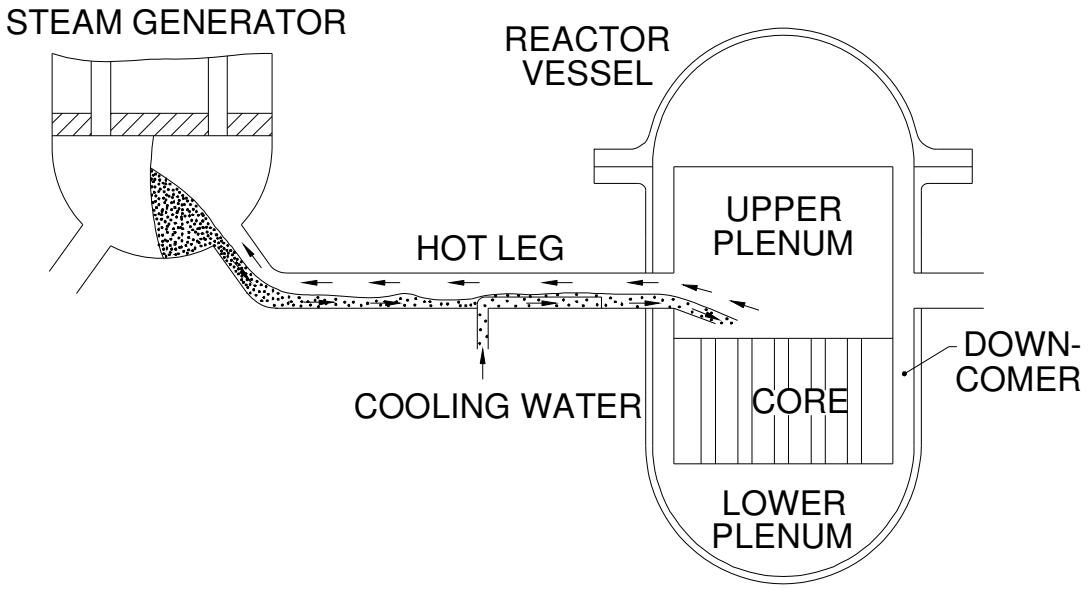

FIG. 17. Counter current flow of steam and water in hot leg of PWR

6. CONCLUSIONS

An account of various phenomena encountered in the natural circulation systems of a nuclear reactor is provided. Thermohydraulic relationships related to these phenomena are given as examples. References are given that contain more relationships covering wider range of parameters to choose from. Some of the phenomena are briefly described. For these phenomena, references are given which will provide deeper insight into these phenomena.

NOMENCLATURE

A - flow area, heat transfer area
A_r - flow area ratio (<1)
A_g - projected grid cross section
Bo - boiling number ($q/G\,h_{fg}$)
c/s - cross section
Co - convection number
C_f - friction coefficient
C_d - drag coefficient
C_p - specific heat
C_v - modified loss coefficient
C_0 - distribution coefficient
D, d - diameter
D_e - equivalent diameter
e - absolute roughness
F - correction coefficient, geometrical factor, enhancement factor
Fr - Froude Number
f - friction factor
f_l - laminar friction factor
f_t - turbulent friction factor
f_R - reference friction factor
G - mass flux
G_{SL} - superficial liquid mass flux ($\rho_L\, j_L$)
g - gravitational acceleration
H - wire pitch
ΔH - subcooling
h - heat transfer coefficient, enthalpy
$h_{fg,}$ h_{LG} - latent heat
I - specific enthalpy
j - volumetric flux
Ja - Jakob number
K - loss coefficient
k - thermal conductivity
L - length
$\dot{m}$ - condensate mass flow rate
N - power
Nu - Nusselt Number
Pr - Prandtl Number
p_t - rod pitch
P, p - pressure, perimeter
p - wetted perimeter
q - heat flux
Q - heat flow rate
Re - Reynolds Number
S - slip ratio, suppression factor
T - temperature
t - thickness
u - velocity
u_R - reference velocity
U - perimeter
V - velocity
v - specific volume
W - mass flow rate, mass fraction
x - mass quality, distance

Z - length, elevation

Greek Symbols

α - void fraction
θ - angle of direction of flow with vertical
β - homogeneous void fraction
Δ - difference
δ - thickness of film
ϕ^2 - two phase friction multiplier
μ - dynamic viscosity
ρ - density
σ - surface tension
χ - Martinelli parameter
ν - kinematic viscosity

Subscripts

a - acceleration, air
av, ave - average
B - bundle
b - bulk
cir - circular
crit - critical
conden- condensation
d - driving
DO - dryout
e - elevation
f - film, frictional
G - vapour
g - gas
GO - gas only
h - hydraulic
H - heated
horiz - horizontal
i - inlet, interface
L - liquid
LO - liquid only
l - local
m - mean
o - outlet
nc - noncondensable
R - relative
s - spacer
sat - saturated
SPF - single-phase flow
TP, TPF- two-phase flow
tot - total
vert - vertical
w - wall

ACKNOWLEDGEMENTS

The author wishes to thank IAEA and its consultants for the valuable suggestions provided. Thanks are also due to Mr. N.K. Maheshwari and Mr. Vikas Jain of RED, BARC for the help rendered in preparing this note.

REFERENCES

[1] INTERNATIONAL ATOMIC ENERGY AGENCY, Thermophysical properties of materials for water cooled reactors, IAEA-TECDOC-949, Vienna (1997).

[2] MOCHIZUKI, Y., ISHII, Y., Study of thermalhydraulics relevant to natural circulation in ATR, Proceedings of the fifth International Topical meeting on Reactor Thermal Hydraulics, vol. I, 127-134 NURETH-5, Salt Lake City, USA (1992).

[3] ARMAND, A.A.., TRESCHEV, G.G., "Investigation of the Resistance During the Movement of Steam-Water mixtures in Heated Boiler Pipes at High Pressure", Izv. Ves. Teplotekh. Inst.; 4, 1-5 (1947).

[4] INTERNATIONAL ATOMIC ENERGY AGENCY, Thermohydraulic relationships for advanced water cooled reactors, IAEA-TECDOC-1203, Vienna (2001).

[5] CHEXAL, B., MAULBETSCH, J., SANTUCCI, J., HARRISON, J., JENSEN, P., PETERSON, C., LELLOUCHE, G., HOROWITZ, J., "Understanding void fraction in steady and dynamic environments", TR-106326 / RP-8034-14, Electric Power Research Institute, 3412 Hillview Avenue, Palo Alto, California (1996).

[6] BLASIUS, H., Mitt. Forsch. Geb. Ing.-Wesen, 131 (1913).

[7] COLEBROOK, C.F., "Turbulent Flow in Pipes with Particular Reference to the Transition Region Between the Smooth and Rough Pipe Laws", J. Inst. Civ. Eng. Lond.; 133-156 (1938).

[8] FILONENKO, G.K., On friction factor for a smooth tube, All Union Thermotechnical Institute (Izvestija VTI, No. 10), Russia (1948).

[9] KNUDSEN, J.G., KATZ, D.L., Fluid Dynamics and Heat Transfer, p. 178, McGraw-Hill Book Company, Inc.; New York (1958).

[10] LEUNG, L.K.H., GROENEVELD, D.C., AUBE, F., TAPUCU, A., New studies of the effect of surface heating on frictional pressure drop in single-phase and two-phase flow, NURETH-3, Grenoble, France (1993).

[11] CICCHITTI, A., LOMBARDI, C., SILVESTRI, M., SOLDAINI, G., ZAVATTARELLI, R., "Two-phase cooling experiments: pressure drop, heat transfer and burnout experiments", Energia Nucleare, 7, 407-425 (1960).

[12] LOTTES, P.A., FLINN, W.S., A Method of Analysis of Natural Circulation Boiling Systems, Nuclear Science Eng.; 19(2), 91-99 (1956).

[13] MARTINELLI, R.C., NELSON, D.B., Prediction of pressure drop during forced-circulation boiling of water, Trans. ASME, 70, 695-702 (1948).

[14] LEUNG, L.K.H., GROENEVELD, D.C., Frictional pressure gradient in the pre- and post-CHF heat-transfer regions, Multiphase flows' 91, Tsukuba, Sept. 24-27, 1991, Tsukba, Japan (1991).

[15] TARASOVA, N.V., et. al., Pressure drop of Boiling Subcooled Water and Steam Water Mixture Flowing in Heated Channels, Proceedings of 3rd Int. Heat Transfer Conf. 178, ASME (1966).

[16] KOEHLER, W., KASTNER, W., Two phase pressure drop in boiler tubes, Two-Phase Flow heat Exchangers: Thermalhydraulic Fundamentals and Design, Editors: S. Kakac, A.E. Bergles E.O. Fernandes, Kluwer Academic Publishers (1988).

[17] VIJAYAN, P.K., SAHA, D., VENKAT RAJ, V., Measurement of pressure drop in PHWR fuel channel with 19 rod bundles (wire-wrap type) at low Reynolds numbers, BARC/I-811 (1984).

[18] PILKHWAL, D.S., VIJAYAN, P.K., VENKAT RAJ, V., Measurement of pressure drop across the junction between two 37 rod fuel bundles for various alignments of the bundles, Proceedings of 19th National Conference on Fluid Mechanics and Fluid Power, IIT, Powai, Bombay, India (1992).

[19] REHME, K., Systematische experimentelle Untersuchung der Abhängigkeit des Druckverlustes von der geometrischen Anordnung für längs durchströmte Stabbündel mit Spiraldraht-Abstandshaltern', KfK, Rep. 4/68-16 (1968).

[20] REHME, K., Druckverlust in Stabbündeln mit Spiraldraht-Abstandshaltern", Forsh. Ing.-Wes.35 Nr.4 (1969).

[21] KAYS, W.M., Convective Heat and Mass Transfer, Tata-McGraw Hill Publishing Company Ltd.; New Delhi (1975).

[22] DIESSLER, G., TAYLOR, M.F., Analysis of Axial Turbulent Flow Heat transfer Through Banks of rods or Tube, Reactor Heat Transfer Conference, TID-7529, Volume 2 (1956).

[23] LOMBARDI, C., CARSANA, C.G., A dimensionless pressure drop correlation for two-phase mixtures flowing upflow in vertical ducts covering wide parameter ranges, Heat and Technology, 10, 125-141 (1992).
[24] MARTINELLI, V., PASTORI, L., AMLETO - A Pressure drop computer code for LWR fuel bundles, RT/ING(73)11, Comitato Nazionale Energia Nucleare (CNEN) (1973).
[25] IDELCHIK, I.E., Hand Book of Hydraulic Resistances, Hemisphere Publishing Company, New York (1986).
[26] REHME K., Pressure Drop Correlations for Fuel Element Spacers, Nuclear Technology, 17, 15-23 (1973).
[27] REHME, K., Pressure Drop of Spacer Grids in Smooth and Roughened Rod Bundles, Nuclear Technology, 33, 313-317 (1977).
[28] CEVOLANI, S., "ENEA Thermohydraulic Data Base for the Advanced Water Cooled Reactor Analysis", 1st Research Co-ordination Meeting of IAEA CRP on Thermohydraulic Relationships for Advanced Water Cooled Reactors, Vienna (1995).
[29] GRILLO, P., MARINELLI, V., Single and Two-Phase Pressure Drops on a 16-ROD Bundle, Nuclear Applications & Technology, 9, 682-693 (1970).
[30] LOTTES, P.A., Expansion losses in two-phase flow, Nuclear Science Eng., 9, 26-31 (1961).
[31] CHISHOLM, D., SUTHERLAND, L.A., "Prediction of Pressure Gradient in Systems During Two-phase Flow", Inst. of Mechanical Engineers, Symposium in Two-phase Flow Systems, Univ. of Leeds (1969).
[32] FITZSIMMONS, D.E., Two-phase pressure Drop in Piping Components, Hanford Laboratory Report", HW-80970 (1964).
[33] ECKERT, E.R.G. and DRAKE JR., R.M., Analysis of Heat & Mass Transfer, McGraw-Hill (1972).
[34] DITTUS, F.W. and BOELTER, L.M.K., University California Publs. Eng., Vol.2, p 443 (1930).
[35] SIEDER, E.N. and TATE, G.E., Heat Transfer and Pressure Drop of Liquids in Tubes, Industrial Engineering Chemistry, 28, 1429-1435 (1936).
[36] COLLIER, J.G., Convective Boiling and Condensation, McGraw-Hill, London (1981).
[37] KANDLIKAR, S.G., A General Correlation for Saturated Two-Phase Flow Boiling Heat Transfer Inside Horizontal and Vertical Tubes, Journal of Heat Transfer, Vol. 112, 219-227 (1990).
[38] CHEN, J.C., "A Correlation for Boiling Heat Transfer to Saturated Fluids in Convective Flow", Industrial and Engineering Chemistry, Process Design and Development, Vol.5, No.3, 322-329 (1966).
[39] FORSTER, H.K and ZUBER, N., Dynamics of Vapour Bubbles and Boiling Heat Transfer, Journal of AIChE, Vol.1, 531-535 (1955).
[40] CHEN, J.C, "A Correlation for Boiling Heat Transfer to Saturated Fluid in Convective Flow", ASME Paper 63-HT-34 (1963).
[41] JENS, W.H., LOTTES, P.A., Analysis of Heat Transfer, Burnout, Pressure Drop and Density Data for High Pressure Water, ANL-4627 (1951).
[42] HEWITT, G.F.; HALL-TAYLOR, N.S., Annular two-phase flow, New York, NY, Pergamon Press (1970).
[43] WEISMAN, J., PEI, B.S., Prediction of Critical Heat Flux in flow boiling at low quality conditions, International Journal of Heat Mass Transfer 26 (1463) (1983).
[44] KUTATELADZE, S.S., Heat Transfer in Boiling and Condensation, USAEC Report AEC-Tr-3770 (1952).
[45] GROENEVELD, D.C. et al., The 2005 Look-Up Table,11th International Topical Meeting on Nuclear Reactor Thermal Hydraulics (NURETH-11), avignon, France, October 2-6, 2005.
[46] TONG, L.S., Boiling crisis and critical heat flux, USAEC Rep. TID-25887 (1972).
[47] YIN, S.T., GROENEVELD, D.C. and WAKAYAMA, M., The effect of radial flux distribution on critical heat flux in 37-rod bundles, ANS Proceedings, 12th National Heat Transfer Conference, Vol. 5, p.277-283 (Minneapolis, July 28-31) (1991).
[48] WONG,Y.L., GROENEVELD, D.C., CHENG, S.C., CHF predictions in horizontal tubes, International Journal of Multi-phase Flow 16 (123) (1990).

[49] PREMOLI, A., FRANCESCO, D., PRINA, A., An empirical correlation for evaluating two-phase mixture density under adiabatic conditions, European two-phase flow group meeting, Milan (1970).
[50] NUSSELT, W., Die Oberflächenkondensation des Wasserdampfes, VDI Z. 60, 541-546, 569-575 (1916).
[51] KUTATELADZE, S.S., Fundamentals of Heat Transfer, Academic Press, New York (1963).
[52] LABUNTSOV, D.A., Heat Transfer in Film Condensation of Pure Steam on Vertical Surfaces and Horizontal tubes, Teploenergetika 4 (1957).
[53] YUNUS, A., Heat transfer: A practical approach, McGraw-Hill, Boston (1998).
[54] CHATO, J.C., "Laminar Condensation inside Horizontal and inclined Tubes." ASHRAE Journal 4, p. 52 (1962).
[55] MAHESHWARI, N.K., PATEL, A.G., VIJAYAN, P.K., SAHA, D. and ARITOMI, M., Evaluation of Free Convective Condensation Modeling in the Presence of Noncondensable Gas, Paper submitted at 5th International Conference on Multiphase Flow, Japan, May 30-June 4 (2004).
[56] UCHIDA, H., OYAMA, A., TOGO, Y., Evaluation of Post-Incident Cooling Systems of Light-Water Power Reactors, Proc. Int. Conf. on peaceful Uses of Atomic Energy 13, 93-102 (1965).
[57] DEHBI, A.A.., "The Effect of Noncondensable Gases on Steam Condensation under Turbulent Natural Convection Conditions", MIT Thesis, Dept. of Nucl. Engg., Massachusetts Institute of Technology (1991).
[58] SIDDIQUE M., The Effects of Noncondensable Gases on Steam Condensation Under Forced Convection Conditions, PhD Thesis, Massachusetts Institute of Technology (1992).
[59] SATISH KUMAR, N.V., MAHESHWARI, N.K., VIJAYAN, P.K., SAHA, D., SINHA, R.K., Studies on the Phenomenon of Thermal Stratification in a Side Heated Enclosures, 6th ISHMT-ASME Heat and Mass Transfer Conference and 17th National Heat and Mass Transfer Conference, IGCAR, Kalpakkam, India (2004).
[60] DAS, S.P., DUTTA, P., Numerical and experimental study of thermal stratification in a side heated cavity, Proceedings of the fourth ISHMT-ASME Heat and Mass Transfer Conference, Pune, India (2000).
[61] AKSAN, N., D'AURIA, F., "Status Report on Relevant Thermal hydraulic Aspects of Advanced Reactor Disigns", OCDE/GD(97)8 (1996).
[62] ZUBER, N., YEH, C.K. GORDAN, On the problem of liquid entrainment, ANL-6244 (1960).
[63] ISHII, M., KATAOKA, I., Mechanistic modelling of pool entrainment phenomenon, International Journal of Heat Mass Transfer, Vol. 27, No.11, pp. 1999-2014 (1984).
[64] MARTIN BERMEJO, J., VAN GOETHEM, G., Sponsored research activities on innovative passive safety systems, Nuclear Engineering and Design 201, 25-40 (2000).
[65] KIGER, K.T., GAVELLI, F., Boron Mixing in Complex Geometries: Flow Structure Details, Nuclear Engineering and Design 208, 67-85 (2001).
[66] BEZRUKOV, Y.A. et.al. Experimental and Numerical Study of the Boron Dilution Incident in VVER-1000 Reactor, Int. Conf. On Nuclear Energy in Central Europe,Bled, Slovenia, Sept. 11-14, 2000.
[67] Rohde, U., Elkin,I., Kalinenko, V., Analysis of Boron Dilution accident for WWER-440 combining the use of the codes DYN3D and SiTap, Nucl. Engg. And Design, 170 (1997) 95-99.
[68] UMMINGER, K., KASTNER, W., LIEBERT, J., MULL, T., Thermal Hydraulics of PwRs with Respect to Boron Dilution Phenomena, Experimental Results from the Test Facilities PKL and UPTF, Nuclear Engg. and Design 204 (2001) 191-203.
[69] SOMCHAI WONGWISES, Two-phase counter current flow in a model of a pressurized water reactor hot leg, Nuclear Engg. and Design, 166, 121-133 (1996).
[70] KIM, HYOUNG TAE, NO, HEE CHEON, Assessment of RELAP5/MOD3.2.2γ against flooding database in horizontal-to-inclined pipes, Annals of Nuclear Energy, 29, 835-850 (2002).